Theory of electrical instabilities of mixed electronic and thermal origin*†

D. M. Kroll‡
The James Franck Institute, University of Chicago, Chicago, Illinois 60637
(Received 4 December 1972)

Switching phenomenon in amorphous semiconductors is analyzed in an electrothermal model. Current-voltage characteristics are obtained from very general mathematical considerations concerning existence, uniqueness, local and global stability, and bifurcation of solutions of the nonlinear equations for temperatures and field. Similar considerations show that in this model switching occurs by the nucleation and growth of a hot spot in the device interior. Detailed results are presented for two specific model systems.

I. INTRODUCTION

In the past few years, interest in amorphous semiconductors has been greatly stimulated by the discovery of reversible switching in certain semiconducting glasses.[1-4] Primary interest has centered on a class of covalently bonded alloys of group -IV, -V, and -VI elements called the chalcogenide glasses. These materials, when encapsuled between two electrodes, exhibit a transition from a high to a low resistance state under the influence of sufficiently high fields.

A typical switching device consists of a thin film of chalcogenide glass 1–10 μ thick sandwiched between two electrodes of refractory material. When voltages are applied, conduction is Ohmic until fields of about 10^4 V/cm. At higher fields, non-Ohmic processes become evident and the current rises exponentially with applied voltage. This non-Ohmic conduction appears to be bulk limited. Switching occurs at fields of about 10^5 V/cm. The actual switching event is extremely rapid (about 10^{-10} sec), but is preceded by a delay time of approximately 10 μsec near threshold. Upon switching, the voltage across the device drops sharply along the load line until a holding voltage of approximately 1 V is reached. Conduction in this state appears to be filamentary in character. The device may be maintained in this state as long as the current does not drop below a critical value. If this holding current is not maintained, the device switches back to the resistive state, attaining its initial resistivity in about 10^{-6} sec. The switching process is entirely reproducible, reversible, and essentially independent of polarity [Fig. 1(a)].[2,5-7]

Some glasses, in particular, those whose compositions lie near the Ge-Te binary eutectic, can be locked into the high-conductance state after switching.[2,8] In these devices, if the electric field is maintained for about a millisecond after switching, the material along the current channel devitrifies and a high density of crystallites forms, creating a bridge of high-conductivity material between the two electrodes. After this devitrification has occurred, the device remains in the low-resistance state even after the electric field is removed [Fig. 1(b)]. It is possible to return

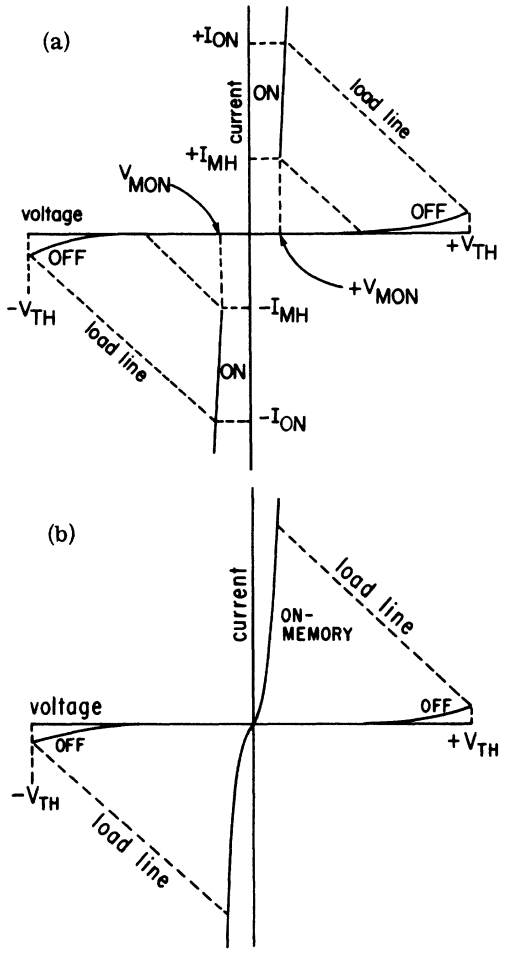

FIG. 1. Schematic current-voltage characteristic of (a) threshold and (b) memory switching devices. Film thickness ~1 μm; contact area ~20-μm diameter; V_{TH} is the threshold voltage; I_{MH} is the minimum holding current; V_{ON} is the operating point after switching.

the device to its high resistance state by applying a sufficiently high, short, current pulse. This reset pulse melts the devitrified material in the current channel. Subsequent rapid cooling of the melt restores the original noncrystalline phase.[9] In both the switching- and memory-type devices, the initial switching mechanism appears to be the same.[2,9]

Several explanations for this switching phenomenon have been suggested. On the one hand, it is argued that a thermal, or more generally, an electrothermal mechanism, dependent only on the electrical and thermal bulk properties of the semiconducting material is sufficient to explain both the switching and the on-state characteristics of the devices.[10–27] On the other hand, several authors have put forward models in which, in the on state, carriers are injected at both electrodes giving a high density of carriers in the valence and conduction bands.[28–31] The conductive state is sustained by double injection provided the applied voltage exceeds the mobility gap. Among the latter group, there exists a difference of opinions concerning the role of thermal effects in establishing the actual switching instability.[32]

It has not yet been possible to decide which of the above suggestions may be correct. Much of the present uncertainty stems from the fact that the problem of thermal switching has not been completely resolved mathematically. Although this subject has a very long history, much of the work has been based on oversimplified or unrealistic models so that no clear-cut detailed understanding of thermal switching has yet developed. Until it becomes clear to what extent a macroscopic theory based solely on the bulk properties of these materials is capable of explaining the observed effect, little progress can be made in determining to what extent nonequilibrium electrode effects, such as space-charge-limited currents or double injection, must be involved. In this paper we shall therefore undertake a detailed investigation of a specific mixed electronic and thermal (MET) theory in an attempt to resolve this uncertainty.[33,34] In Sec. II of this paper we shall present a general description of the MET theory, discuss the relevant material parameters, equations, and typical device geometries. In Sec. III, we shall discuss several simplified but still appropriate model systems. The results of our calculations of, e.g., current-voltage characteristics for a restricted one-dimensional case will be presented in Sec. IV, while in Sec. V we report corresponding results for three dimensions. Section VI contains a discussion of the temporal stability of the steady-state solutions we have obtained in Secs. IV and V. A clear-cut picture of the content of the MET theory of switching emerges from these results; it is discussed in Sec. VII together with predictions and conclusions following from it.

II. GENERAL DESCRIPTION OF MET, MATERIAL PARAMETERS, EQUATIONS, AND DEVICE GEOMETRIES

A. Description and equations

The thermal theory of breakdown is a very old subject, with a literature dating back to at least the early 1920's. We cannot even hope to mention most of the papers in this field, but shall be content with describing the application of the general theory to the problem of interest, only citing past work whenever appropriate.[35–38]

The particular attractiveness of electrothermal theories lies in the fact that they permit a description of the system in mathematically closed form, permitting, at least in principle, quantitative solution. The theory is entirely classical and macroscopic in content, requiring a knowledge only of the field and temperature dependence of the glasses' heat capacity and thermal and electrical conductivities.

A proper treatment of the theory begins with the thermodynamic constitutive equations relating the thermal and electrical currents to the thermodynamic driving forces. In principle, thermoelectric and Peltier effects should be included. The chalcogenide glasses we are interested in possess Seebeck coefficients of the same order of magnitude as crystalline semiconductors.[39] However, numerical calculations performed by Kaplan and Adler indicate that Peltier and thermoelectric effects are negligible even at very large current densities and temperature gradients so that it appears reasonable to ignore these effects.[25] In any effect, their omission would not change any of the qualitative predictions of the theory, contributing perhaps only to a slight increase in the predicted holding voltages. If we take the Seeback coefficient to be zero, we have for the heat current

$$\vec{j}_q = -K\vec{\nabla}T$$

and electrical current

$$\vec{j} = \sigma\vec{E},$$

where K and σ are the thermal and electrical conductivities, respectively.

In addition, it is only required to utilize the conservation of energy or entropy and Maxwell's equations to specify the problem completely. In the present case, these relations reduce to

$$C\frac{\partial T}{\partial t} = \vec{\nabla}\cdot K\vec{\nabla}T + \vec{j}\cdot\vec{E}, \tag{1}$$

$$\vec{j} = \sigma\vec{E}, \tag{2}$$

Maxwell's equations. (3)

Equations (1)–(3) complete description of the theory once $K(T, E)$ and $\sigma(T, E)$ are known and proper boundary conditions on T and $\vec{E}$ or $\vec{j}$ are specified.

B. Material parameters

Memory and switching devices can be constructed from a wide variety of chalcogenide-based glassy semiconductors. These materials may be prepared in their amorphous form in the bulk and their physical properties determined. Typical of the threshold switching materials are Te-As-Ce alloys such as $Te_{50}As_{30}Si_{10}Se_{10}$,[8] while memory switching materials are commonly Ge-Te mixtures near the Ge-Te eutectic such as $Ge_{15}Te_{81}Sb_2S_2$.[8,40] Switching has even been observed in selenium and Se-Te mixtures a few hundred degrees above their melting points.[41–43]

The glasses which exhibit stable switching characteristics generally have conductivities between 10^{-5} and 10^{-7} Ω^{-1} cm^{-1} at room temperature. In a broad range about room temperature the electrical conductivity exhibits an "intrinsic"-type behavior with an activation energy on the order of 0.5–0.6 eV. At higher temperatures the conductivity behaves anomolously, increasing more rapidly with increasing temperature, starting at the softening temperature. At the highest temperatures in the liquid, the conductivities tend to saturate at about 10^2 to 10^3 Ω^{-1} cm^{-1}. This behavior was observed to hold quite generally for the Ge-Sb-Se and Ge-As-Se systems of glasses studied by Haisty and Krebs,[44] in the Se-Te liquid systems studied by Perron,[45] and in many other systems.[14,46,47] In the present paper we use electrical conductivity data for $Ge_{15}Te_{81}X_4$ (X a multielement additive) kindly supplied by J. Evans (Fig. 2).

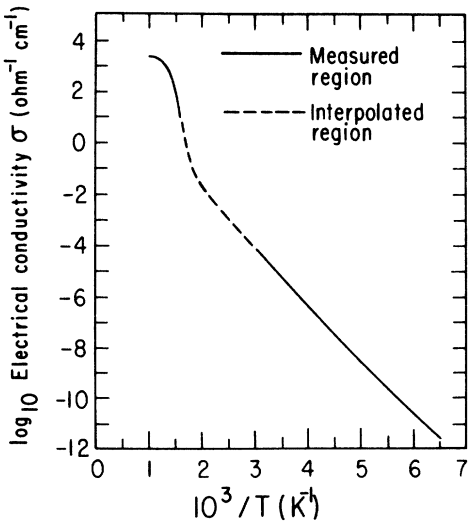

FIG. 2. Electrical conductivity of $Ge_{15}Te_{81}X_4$.

At high fields the chalcogenide glasses also exhibit a field dependence of the conductivity, generally expressed in the form

$$\sigma(T, E) = \sigma(T)\, e^{|E|/E_0},$$

where E_0 is approximately 10% of the critical field for switching glasses and somewhat greater for materials with high tellurium content.[26,48,49] In general, the temperature dependence of E_0 is not known, but the field dependence of the conductivity is expected to decrease at higher temperatures, at least in the molten state, where these materials become more metallic and the temperature dependence of σ flattens out.

It will be seen that this field dependence is essential in obtaining results resembling the observed switching effect. For $Ge_{15}Te_{81}X_4$ we believe E_0 to lie in the range $(1–3)\times10^4$ V/cm at room temperature.

Finally, the thermal conductivity of chalcogenide glasses is very low at room temperature, generally on the order of 2–3 mW/cm °K. The thermal conductivity K of $Ge_{15}Te_{81}X_4$ has been measured by de Neufville to be 2.2 mW/cm °K at room temperature[50] and appears to remain constant until temperatures at which the electronic contribution becomes significant, somewhere above the softening temperature of the glass. Perron has measured the electronic component of K in Se-Te alloys at high temperatures and found that it obeys a Wiedemann-Franz law with a Lorentz number of 2.45×10^{-8} WΩ/°K^2.[51] We expect a somewhat similar behavior in the glasses of interest, so that

$$K = K_l + L\sigma T .$$

The relevant semiconductor material parameters are presented in Table I.

C. Device geometries

Figure 3 shows an exploded view of a typical switching device. The essential geometric features of the device are (i) its sandwich configuration, and (ii) that switching is limited to a disc of semiconducting material 20 μ in diameter. The upper Molybdenum electrode is 1.2 μ thick and is overlaid with a layer of aluminum 5 times as thick for improved electrical conductivity and heat sinking. The single-crystal silicon substrate serves as an excellent heat sink. This configuration possesses a capacitance of about 1.5 PF and experimentally offers stable reproducible switching

TABLE I. Material parameters.

$E_0 = (1–3)\times10^4$	V/cm
$K_l = 2-4$	mW/cm °K
$L = 2.45\times10^{-8}$	WΩ/°K^2

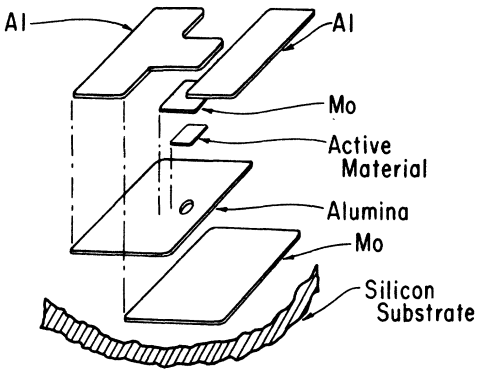

FIG. 3. Exploded view of thin film sandwich device [Neale (Ref. 52)].

characteristics.[52]

There are many variations on this specific configuration, but all geometries commonly used possess these several essential features: The glass is deposited as a thin film between electrodes whose thermal conductivities are approximately 1000 times greater than that of the glass. The semiconducting film is generally 0.5–2 μ thick, and the lateral dimensions over which switching is permitted are delimited by the electrodes to be a disc 20–40 μ in diameter. There is essentially no radial coupling to a heat sink, so that virtually all the cooling is provided by the electrodes, and heat flow is nearly parallel to the current flow.

III. APPROPRIATE MODEL SYSTEMS

We shall investigate solutions of the system [Eqs. (1)–(3)] in two separate idealized models.

A. Model *A*

In this case we attempt to approximate as realistically as possible the actual device geometry and boundary conditions. The region in which Eqs. (1)–(3) hold will be a disc 1 μ thick and 20 μ in diameter. We use cylindrical coordinates r, ϕ, z, but shall restrict ourselves to cylindrically symmetric solutions $T(r, z)$, $\vec{j}(r, z)$.

The boundary conditions appropriate to the actual device are no heat loss or current flow through the sides of the disc,

$$\left.\frac{\partial T}{\partial r}\right|_R = j_r|_R = 0 , \tag{4}$$

and balance of both heat and current flow at the electrodes,

$$K\frac{\partial T}{\partial z} = K_e \left.\frac{\partial T}{\partial z}\right|_e , \quad z = \pm \tfrac{1}{2} d$$
$$\vec{j} = \vec{j}_e , \tag{5}$$

where the right-hand side of (5) is evaluated in the electrode.

We suppose that the conductivity of the electrodes is much greater than that of the semiconductor, so that the electrodes may be taken to be surfaces of constant potential. In addition, we ignore Joule heating within the electrodes, a slightly worse approximation, particularly at the high-current densities attained in the post switching state, and assume that K_e is a constant.

We complete specification of the boundary conditions by taking the electrodes to be cylinders of radius R and height h_e, requiring that no heat conduction takes place out of their sides, and that the outer surfaces of the electrodes are locked at ambient, T_0. This last assumption is not unduly restrictive; by varying h_e over realistic ranges we can be sure of bracketing the actual device heat loss to the electrodes. In fact, some devices are constructed with pyrolytic graphite electrodes which possess highly anisotropic conduction properties. The high-conductivity direction is placed perpendicular to the film surface, so that most cooling is in the z direction. In calculations we shall take h_e in the range of 10–40 μ and use $K_e = 2.4$ W/cm °K, the value of the thermal conductivity of aluminum.

We note that with these approximations, the first equation in (5) becomes

$$K\frac{\partial T}{\partial z} + \alpha T = \alpha T_0 , \tag{6}$$

where $\alpha = K_e/h_e$, for radially uniform solutions of Eqs. (1)–(3).

In order to simplify analysis and more clearly illustrate some of our results, it is useful to study the following simplified model.

B. Model *B*

If in Eq. (1) we approximate axial heat loss by the effective cooling term

$$-(8K/d^2)(T - T_0),$$

where T_0 is ambient, and ignore the axial dependence of the temperature and current, the thermal balance equation simplifies to[53]

$$C\frac{\partial T}{\partial t} = \frac{1}{r}\frac{\partial}{\partial r}\left(rK\frac{\partial T}{\partial r}\right) - \frac{8K}{d^2}(T - T_0) + \frac{j^2}{\sigma} . \tag{7}$$

This equation is a relatively simple parabolic partial differential equation, independent of z.

We again specify $R = 10$ μ and $d = 1$ μ as in Model *A*. We specify that no heat loss or current flow takes place out of the edges of the semiconducting disc,

$$\left.\frac{\partial T}{\partial r}\right|_R = j_r|_R = 0$$

and complete specification of the boundary conditions by assigning a value I to the total current through the device,

$$I = 2\pi \int_0^R r\,dr j .$$

A very useful consequence of these assumptions is that the electric field E only has a component in the z direction and is independent of r in the steady state.

The primary usefulness of model B lies in investigating the implications of thermally induced negative resistance.

It has been pointed out to us recently that solutions in a similar model system have been investigated by Spenke and co-workers for the specific choice of $\sigma(T) = 1 + T^2$.[54-57] In the context of Ovshinsky's discoveries, Croitoru and co-workers,[23,24] Thomas and Male,[14] and Shousha[27] have investigated solutions of (7) numerically. We shall comment further on these works later in the paper.

IV. ONE-DIMENSIONAL RESULTS

Consider the steady-state version of the system (1)–(3) in both models A and B. This system of equations, with the various boundary conditions discussed, constitutes a well-defined boundary-value problem, and it may be proven that solutions exist for all I-V.[58] One can impose a given total current I:

$$I = 2\pi \int_0^R j_z(r, z) r\,dr \quad (\text{any } z),$$

solve the system (1)–(3) to establish V, and thus derive the whole I-V characteristic, at least in principle.

Before attempting to investigate the properties of general steady-state solutions to Eqs. (1)–(3), it is instructive to consider a certain subclass of solutions. It is clear that for the boundary conditions imposed, solutions which satisfy the time-independent system corresponding to Eqs. (1)–(3) or (7), in which the r coordinate is suppressed, will be solutions to the full system. We shall investigate some of the properties of these radially independent solutions first.

A. Model B

Radially independent solutions of the steady-state version of (7) will obey the nonlinear algebraic relation

$$-(8K/d^2)(T - T_0) + \sigma(T, E)E^2 = 0 . \tag{8}$$

The current is given by $I = \pi R^2 \sigma(T, E)E$ and the potential is given by $V = Ed$.

It is clear that a solution to Eq. (8) exists for any positive I or V. Also,

$$\frac{dI}{dT} = \pi R^2 \left[\frac{\partial \sigma}{\partial T} E + \left(1 + \frac{E}{E_0}\right) \sigma(T, E) \frac{\partial E}{\partial T} \right]$$

$$= \pi R^2 \left(\left\{ \sigma \frac{\partial \sigma}{\partial T} E^2 + \sigma \left(1 + \frac{E}{E_0}\right) 8K/d^2 + \frac{\sigma E^2}{K} L \left[\sigma \frac{\partial \sigma}{\partial T} T + \sigma^2 \left(1 + \frac{E}{E_0}\right) \right] \right\} \left[\sigma E \left(2 + \frac{E}{E_0}\right) - \frac{L\sigma T}{K} \frac{\sigma E^2}{E_0} \right]^{-1} \right) > 0 ,$$

where L is the Lorentz number, since, taking d/dT of (8),

$$\frac{\partial E}{\partial T} = \left[\frac{8K}{d^2} - \frac{\partial \sigma}{\partial T} E^2 + \frac{\sigma E^2}{K} L \left(\frac{\partial \sigma}{\partial T} T + \sigma \right) \right] \times \left[\sigma E \left(2 + \frac{E}{E_0}\right) - \frac{L\sigma T}{K} \frac{\sigma E^2}{E_0} \right]^{-1}$$

and $L\sigma T < K$. Therefore, I is a monotonically increasing function of T, and Eq. (8) has a unique solution for any I. Furthermore,

$$\frac{dE}{dI} = \frac{dE}{dT} \frac{dT}{dI}$$

$$= \left[\frac{8K}{d^2} - \frac{\partial \sigma}{\partial T} E^2 + \frac{\sigma E^2}{K} L \left(\sigma + \frac{\partial \sigma}{\partial T} T \right) \right] \times \left\{ \sigma \frac{\partial \sigma}{\partial T} E^2 + \sigma \left(1 + \frac{E}{E_0}\right) \frac{8K}{d^2} + \frac{\sigma E^2}{K} L \left[\sigma \frac{\partial \sigma}{\partial T} T + \sigma^2 \left(1 + \frac{E}{E_0}\right) \right] \right\}^{-1} ,$$

so that $dE/dI < 0$ on the I-V characteristic determined by solutions of (8), provided

$$\frac{8K}{d^2} - \frac{\partial \sigma}{\partial T} E^2 + \frac{\sigma E^2}{K} L \left(\sigma + \frac{\partial \sigma}{\partial T} T \right) < 0 .$$

In this case there exists a portion of the I-V characteristic on which $dV/dI < 0$, and the current is not a single-valued function of the field. The temperatures which delimit this break-back region are determined as the simultaneous solutions of (8) and

$$\frac{8K}{d^2} - \frac{\partial \sigma}{\partial T} E^2 + \frac{\sigma E^2}{K} L \left(\sigma + \frac{\partial \sigma}{\partial T} T \right) = 0 . \tag{9}$$

For temperatures below 500 °K, the thermal conductivity K is independent of temperature, so that (9) reduces to

$$\frac{8K}{d^2} - \frac{\partial \sigma}{\partial T} E^2 = 0 \tag{10}$$

and the temperature T_1 at the voltage maximum V_1 is given as a solution of

$$-\sigma(T) + \frac{\partial \sigma(T)}{\partial T}(T - T_0) = 0 . \tag{11}$$

For the electrical conductivity given in Fig. 2, Eq. (11) has the solution $T_1 \approx 20°$ above ambient (295 °K). T_1 is independent of sample thickness and strength of the field dependence of σ in this model.

Returning to (9) we find that the temperature T_2, at the point where dV/dI turns positive again, is $\lesssim 450°$ above ambient and is weakly dependent on the sample thickness.[59] There are two primary reasons for this relatively low value of T_2; most important is the anomalous increase, and subsequent saturation, of σ at about 750 °K. Also important is the increase in K by more than an order of magnitude at these temperatures. If K were constant and σ were to continue to exhibit an activated temperature dependence well into the melt, T_2 would be predicted by this model to be ~2500 °K. We shall see later that T_2 is approximately the temperature we expect in the conducting channel which exists in the post switching state.

If T_0 is great enough, about 625 °K in this case, no simultaneous solutions to Eqs. (8) and (9) exist and we lose the break-back portion of the I-V characteristic. In fact, for ambient temperatures 50–75 °K below this value, the I-V characteristic is very nearly vertical for over a decade of current near the voltage turnaround point.

Figure 4 contains a graph of the break-back field $E_1 = V_1/d$ versus sample thickness for fixed $E_0 = 3.7 \times 10^4$ V/cm and ambient temperature $T_0 = 295$ °K. We see that for samples sufficiently thick that $V_1 \ll 2dE_0$, $E_1 \sim 1/d$ holds; for thin samples for which $V_1 \gg 2dE_0$, E_1 increases more slowly with $1/d$, becoming only logarithmically dependent on the thickness.

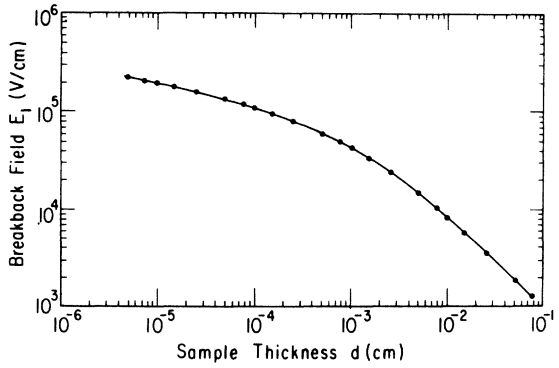

FIG. 4. Break-back field E_1 as a function of sample thickness d calculated using model B. Ambient temperature $T_0 = 295$ °K, $E_0 = 3.7 \times 10^4$ V/cm, and $K_l = 4$ mW/cm °K.

This behavior of E_1 in the two limiting cases may be seen by writing out the field dependence in (8) explicitly. Since K is constant near T_1, Eq. (8) becomes

$$-8K(T_1 - T_0) + \sigma(T_1) V_1^2 e^{V_1/dE_0} = 0 . \tag{12}$$

Let

$$V_a^2 = \frac{8K(T_1 - T_0)}{\sigma(T_1)}, \quad X = \frac{V_1}{2dE_0}, \quad X_a = \frac{V_a}{2dE_0} .$$

Then, Eq. (12) reduces to $X = X_a e^{-X}$ or, taking the logarithm of both sides,

$$X = \ln X_a - \ln X . \tag{13}$$

We use (13) to determine the small-d limiting behavior of E_1. Iterating on (13), using $X = 1$ as a first approximation, we have

$$X^{(1)} = \ln X_a ,$$

$$X^{(2)} = \ln X_a - \ln \ln X_a .$$

This iteration scheme converges if $\ln X_a \gg \ln \ln X_a$, or equivalently, if $X_a \ggg 1$; in this case, $X \sim \ln X_a$. Therefore we see that if $V_a \gg 2dE_0$ (small-d limit),

$$E_1 \xrightarrow[d \to 0]{} 2E_0 \ln\left[\frac{1}{2dE_0}\left(\frac{8K(T_1 - T_0)}{\sigma(T_1)}\right)^{1/2}\right]. \tag{14}$$

In the small-d limit, then, the turnaround field varies as the logarithm of d. To investigate the large-d behavior, let $y = V_1/V_a$, and $y_0 = 2dE_0/V_a$ so that (12) becomes

$$y = e^{-y/y_0} . \tag{15}$$

If $y_0 \gg 1$ we see that iteration on (15) converges rapidly. Letting $y^{(0)} = 1$, we have

$$y^{(1)} = e^{-1/y_0} \approx 1 - 1/y_0 .$$

So that if $y_0 \gg 1$, or equivalently, $V_a \ll 2dE_0$, we have

$$V_1 \sim V_a$$

and

$$E_1 \xrightarrow[d \to \infty]{} V_a/d . \tag{16}$$

The ambient temperature dependence of V_1 in these two limits follows immediately from (14) and (16). From (11) and the fact that $\sigma(T) = \sigma_0 e^{-C/T}$ ($C \approx 5200$ °K) near room temperature, we have

$$T_1 - T_0 = T_1^2/T_0 . \tag{17}$$

Substituting in (14),

$$E_1 \xrightarrow[d \to 0]{} 2E_0 \ln\left[\frac{1}{2dE_0} \frac{T_1 e^{C/2T_1}}{\sigma_0}\left(\frac{8K}{C}\right)^{1/2}\right]$$

$$\approx 2E_0\left\{\ln\left[\left(\frac{8K}{C}\right)^{1/2}\frac{1}{2\sigma_0 dE_0}\right]+\ln T_0+\frac{C}{2T_0}\right\},$$

to 7% accuracy at ambients near room temperature. For $d\to\infty$, we use (16) so that

$$E_1 \xrightarrow[d\to\infty]{} \left(\frac{8K(T_1-T_0)}{\sigma(T_1)}\right)^{1/2} = \left(\frac{8K}{\sigma_0 C}\right)^{1/2} T_1 e^{-C/2T_1}$$

$$\approx \left(\frac{8K}{\sigma_0 C}\right)^{1/2} T_0 e^{-C/2T_0}$$

to (20–30)% accuracy at ambients near room temperature, so that the temperature dependence of E_1 becomes almost exponential at large thickness. Similar results have been noted by Warren and Male,[13] Chen and Wang,[15] and Mott.[32] Figure 5 contains a plot of E_1 vs T_0 for $d=10^{-4}$ cm and $E_0=3.7\times10^4$ V/cm.

Another point worth noting is the way that V_1 scales with E_0. Equation (12) contains d and E_0 only in the form of their product, so that the effect on V_1 of decreasing E_0 is the same as that of decreasing d. The limits discussed above for the thickness dependence of E_1 will be reached for a range of device thicknesses, depending upon the size of E_0. As either E_0 or $d\to 0$, $V(T_1)\to V(T_2)$ and the break-back portion of the I-V characteristic becomes vertical.

The I-V characteristic determined by the solution of (8) with $E_0=3.7\times10^4$ V/cm is shown in Fig. 6.

B. Model A

In one dimension, the steady-state form of the system [Eqs. (1)–(3)] becomes, under the assumptions of model A,

$$\frac{d}{dz}\left(K\frac{dT}{dz}\right)+jE=0, \tag{18}$$

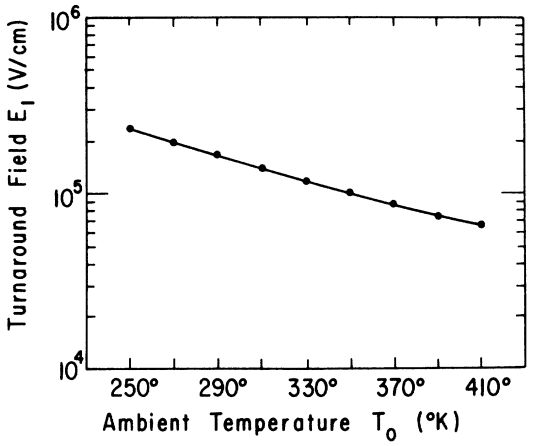

FIG. 5. Break-back field E_1 as a function of ambient temperature T_0 calculated using model B. Sample thickness $d=1$ μm, $E_0=3.7\times10^4$ V/cm, and $K_l=4$ mW/cm °K.

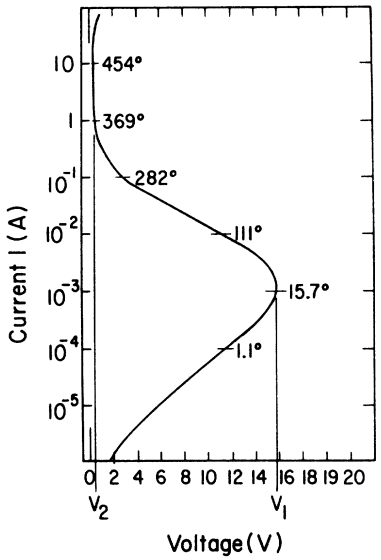

FIG. 6. Current-voltage characteristic determined by solution of Eq. (8) using $T_0=295$ °K, $d=1$ μm, $R=10$ μm, $E_0=3.7\times10^4$ V/cm, $K_l=4$ mW/cm °K, and $L=2.45\times10^{-8}$ W Ω/°K^2. Temperatures listed are °K above ambient.

$$\sigma(T,E)=\sigma(T)\,e^{|E|/E_0}, \tag{19}$$

$$j=\sigma(T,E)E, \tag{20}$$

in domain $D=(-\frac{1}{2}d,\frac{1}{2}d)$, and

$$K\frac{dT}{dz}+\alpha T=\alpha T_0. \tag{21}$$

j is independent of z and the current density is uniform across the cylindrical conducting region. We write E for $d\phi/dz$.

It has been known for quite some time that if σ does not depend upon E and the electrodes are infinite heat sinks, so the $T(\pm\frac{1}{2}d)=T_0$, the I-V characteristic determined by the solutions of Eqs. (18)–(21) does not possess any negative resistance segment.[25,55,60] What is happening is that the field concentration in the cool resistive region near the electrodes offsets the resistance drop in the hot region, never permitting the device resistance to decrease rapidly enough as a function of applied voltage for turnaround to occur. With the presence of a field dependence of the electrical conductivity, this result is no longer valid. The field dependence of σ tends to flatten the field profile across the film,[22] permitting a decrease in the device resistance as the interior is heated. For a field dependent σ the I-V characteristic obtained by the solution of Eqs. (18)–(20) with either perfect-cooling boundary conditions or (21) always possesses a region in which $dV/dI<0$ for normal ambient temperatures.

The I-V characteristic obtained by numerical

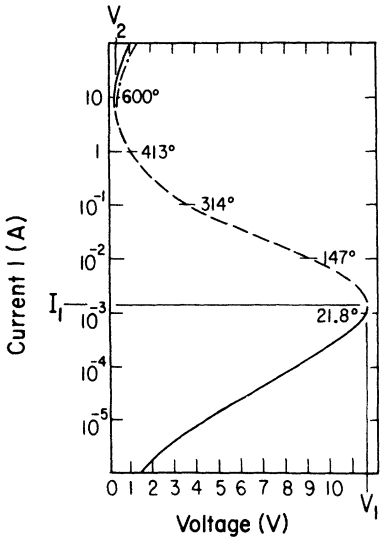

FIG. 7. Current-voltage characteristic obtained by solution of system (18)–(21) using $d=1\,\mu$m, $R=10\,\mu$m, $K_l=2.2$ mW/cm °K, $E_0=2.5\times10^4$ V/cm, $L=2.45\times10^{-8}$ WΩ/°K^2, $K_e=2.4$ W/cm °K, and $h_e=20\,\mu$m. Temperatures listed are peak internal temperatures in °K above ambient, $T_0=295$ °K. Solid curve: stable; dashed curve: unstable; dash-dot curve: asymptotic extrapolation.

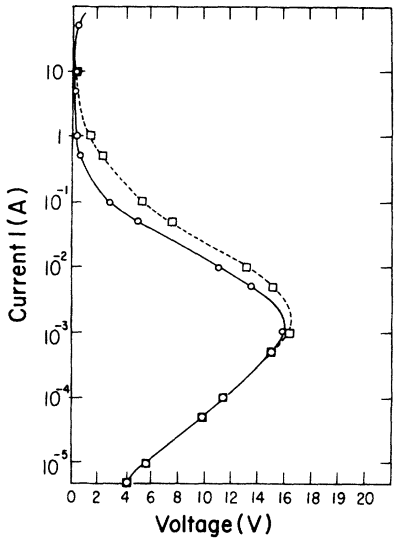

FIG. 8. Comparison of current-voltage characteristics determined by the solution of system (18)–(21) using $h_e=20\,\mu$m and $K_e=2.4$ W/cm °K (model A: dashed curve), and Eq. (8) (model B: solid curve), for the same values of ambient temperature $T_0=295$ °K, E_0, K_l, and L.

solution of Eqs. (18)–(21) for $d=1\,\mu$, $K_l=2.2$ mW/cm °K, $E_0=2.5\times10^4$ V/cm, and $h_e=20\,\mu$, is presented in Fig. 7. The temperatures listed are peak internal temperatures at various operating points. The peak central temperature at V_1 is about 20° above ambient, while at the voltage minimum V_2, it is about 600° above ambient. The temperature profile at V_2 is relatively flat across 95% of the device, only decreasing sharply at the electrodes. Again, as with model B, the peak central temperature at V_2 lies near the point at which σ flattens out as a function of T. This is to be expected, since further heating of the device interior will not decrease the material's resistivity, so that the differential resitance must become positive when most of the central region attains temperatures in this range. For ambient temperatures on the order of 600 °K it is clear, for this reason, that the I-V characteristic will lose its segment of negative resistance.

We found V_2 to lie between ~0.2 and ~0.36 V for h_e in the range 10–40 μ. At V_2, essentially all the potential drop occurs at the electrodes. The electric field attains values of approximately 1.5×10^5 V/cm right at the electrodes and drops rapidly to values three orders of magnitude smaller at the device interior.

As with Eq. (8), it may be shown that for the system (18)–(21), only this one branch of the I-V characteristic exists, and that it is uniquely determined as a function of I (Appendix A). In fact, for typical values of E_0, the I-V characteristics determined by solutions of Eqs. (8) and (18)–(21) are very similar, essentially overlapping at low-current densities (Fig. 8). This was found to be true for all device thicknesses, so that one expects the behavior of V_1 as a function of d and ambient temperature to be essentially the same for both model systems. This is supported by the results presented in Table II concerning the dependence of V_1 on device thickness d.

As in model B, it can be shown that the results concerning the thickness and E_0 dependence of V_1 are directly related. In the temperature range of interest, K is constant; let $x\in(-\frac{1}{2},\frac{1}{2})$ so that $z=xd$,

TABLE II. Dependence of turnaround voltage V_1 on device thickness d for model A. $K_l=2.2$ mW/cm °K, $E_0=2.5\times10^4$ V/cm, $h_e=20\,\mu$m.

d (cm)	V_1 (V)	I_1 (A)
2.5×10^{-5}	4.035	1.1×10^{-2}
5×10^{-5}	6.94	4×10^{-3}
10^{-4}	11.58	1.3×10^{-3}
5×10^{-4}	33.12	1.1×10^{-4}
10^{-3}	48.25	4.0×10^{-5}
5×10^{-3}	92.1	5.2×10^{-6}
10^{-2}	110.2	2.5×10^{-6}
5×10^{-2}	141.0	6.5×10^{-7}
10^{-1}	149.6	4.1×10^{-7}

and let $T(\pm \frac{1}{2}d) = T_0$. Then (18) becomes, if we make the change of variables $x = z/d$,

$$K\frac{d^2T}{dz^2} + \sigma(T)\left(\frac{d\phi}{dz}\right)^2 e^{|\frac{d\phi}{dz}|/dE_0} = 0, \qquad T(\pm\tfrac{1}{2}) = T_0. \tag{22}$$

Therefore, for a given V, solutions of (18) all scale in terms of one parameter, dE_0, and not with either of these variables independently, so that V_1 depends only on the product dE_0. The effect upon V_1 is the same whether either E_0 or d is increased or decreased.

Finally, V_1 was found to depend only very weakly on the temperature boundary conditions, varying between 11.8 and 11.4 V between the limits of perfect cooling and $h_e = 40\ \mu$, so that the previous result holds to a high degree of accuracy even if the electrodes are not locked at ambient. For none of the boundary conditions used was there significant heating of the electrodes at these low-power densities.

V. THREE-DIMENSIONAL RESULTS

In general, for solutions of either the steady-state form of (7),

$$\frac{1}{r}\frac{d}{dr}\left(rK\frac{dT}{dr}\right) - \frac{8K}{d^2}(T - T_0) + \sigma(T, E)E^2 = 0, \tag{23}$$

$$T(0)\ \text{(finite)}, \quad \left.\frac{dT}{dr}\right|_R = 0, \tag{24}$$

$$I = 2\pi\int_0^R r\,dr\,\sigma(T, E)E \tag{25}$$

or the appropriate steady-state form of Eqs. (1)–(3) for model A,

$$\vec{\nabla}\cdot(K\vec{\nabla}T) + \vec{j}\cdot\vec{E} = 0, \tag{26}$$

$$\vec{\nabla}\cdot\vec{j} = 0, \tag{27}$$

$$\vec{\nabla}\times\vec{E} = 0, \tag{28}$$

$$\vec{j} = \sigma(T)E\,e^{|E|/E_0}, \tag{29}$$

$$x \in D = \{(r, \phi, z)\,|\,0 \le r < R,\ 0 \le \phi < 2\pi,\ -\tfrac{1}{2}d < z < \tfrac{1}{2}d\},$$

$$j_r\big|_R = \left.\frac{\partial T}{\partial r}\right|_R = 0, \quad K\left.\frac{\partial T}{\partial z}\right|_{\pm d/2} = K_e\left.\frac{\partial T}{\partial z}\right|_e, \tag{30}$$

$$j_r(\pm\tfrac{1}{2}d, r) = 0, \qquad I = 2\pi\int_0^R r\,dr\,j_z(r, z), \tag{31}$$

it is not possible to prove a uniqueness theorem. As we know that unique radially uniform solutions exist in both cases, the existence of additional, radially nonuniform stationary solutions is implied. In fact, we shall see that for both of these systems additional branches of the I-V characteristic corresponding to radially dependent temperature and current distributions bifurcate from points along the break-back portion of the I-V characteristic determined by the radially uniform solutions. In this section, we shall establish criteria for the existence of these solutions and consider their dependence on device dimensions, material parameters, and boundary conditions.

A. Model *B*

1. Phase-plane analysis

Considerable qualitative information concerning solutions of Eq. (23) may be obtained by performing a phase-plane analysis.

Consider the equation

$$\frac{d^2u}{dr^2} + \frac{1}{r}\frac{du}{dr} - \frac{8}{d^2}(u - u_0) + \lambda\sigma(u) = 0, \tag{32}$$

in which λ is a parameter. This is simply Eq. (23) with K taken to be constant, $u = T$, and $\lambda = (1/K) \times E^2 e^{E/E_0}$. Defining $v = du/dr$, we can write (32) as a pair of first-order equations,

$$v = \frac{du}{dr}, \tag{33}$$

$$\frac{dv}{dr} = -\frac{1}{r}\frac{du}{dr} + \frac{8}{d^2}(u - u_0) - \lambda\sigma(u) \tag{34}$$

and can regard any solution as the motion of a representative point with coordinates (u, v) in a phase plane.[61] We define an "energy" A by

$$A = \tfrac{1}{2}v^2 - (8/d^2)(\tfrac{1}{2}u^2 - uu_0) + \lambda\int^u \sigma(x)\,dx$$

in analogy with the dynamical counterpart. We then have

$$\frac{dA}{dr} = -\frac{1}{r}v^2 \le 0,$$

so that A decreases as a function of r, and solutions of (32) cut "downhill," across lines of constant A as r increases.

First consider Eq. (32) with $\lambda = \lambda^* \in (\lambda_1, \lambda_2)$, where λ_1 and λ_2 are the pair of solutions to the system (see Sec. IV)

$$-\frac{8}{d^2} + \frac{\partial\sigma}{\partial u}\lambda = 0, \tag{35}$$

$$-(8/d^2)(u - u_0) + \lambda\sigma(u) = 0. \tag{36}$$

Figure 9(a) contains a sketch of the set of solution points to (36), $u(\lambda)$. We denote the points at which the line $\lambda = \lambda^*$ intersects the $u(\lambda)$ curve by a, b, and c.[62] Figure 9(b) contains a sketch in the phase plane of lines of constant A for this value of $\lambda = \lambda^*$. Several classes of phase-plane trajectories are possible.

Since we require that $v = du/dr = 0$ at $r = 0$, solutions must start on the u axis. If the $(1/r)\,du/dr$ term were not present in (34), these would be no loss of "energy" and the representative point would move along lines of constant A in the sense indicated by the arrows. This sense is determined by

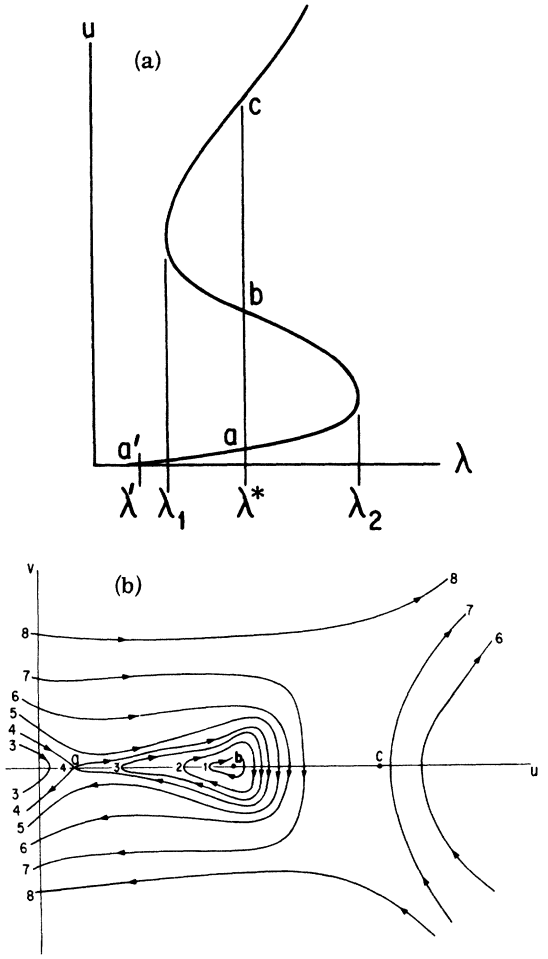

FIG. 9. (a) Sketch of solution points $u(\lambda)$ to Eq. (36). (b) Constant A level curves in the phase plane for $\lambda = \lambda^* \in (\lambda_1, \lambda_2)$. Numerical values of A in arbitrary units.

(33), taking dr positive. Ignoring the damping term, we see that for $u(0) = a$, b, or c, $u(r)$ is a constant, and we have the three radially independent solutions of (36). If $u(0) > c$, $du/dr > 0$ for all r and $u(r) \to \infty$ as $r \to \infty$. Also, if $u(0) < a$, $du/dr < 0$ for all r and $u(r) \to -\infty$ as $r \to \infty$.

But if $u(0)$ lies inside the level curve 4, the solution oscillates about b, and if $u(0)$ lies below c and to the right of level curve 4, the solution drops rapidly at first, almost flattens out and then eventually approaches $-\infty$ as $r \to \infty$.

We can now obtain a qualitative idea of possible solutions to (32) for $\lambda = \lambda^*$. We seek to determine the type and number of possible solutions for a given boundary condition at $r = R$.

a. $(du/dr)|_R = 0$. In this case it is clear that for any $u(r)$ such that $u(0)$ lies either to the left of a or to the right of c, the boundary condition $(du/dr)|_R = 0$ can never be satisfied. But, suppose $u(0)$ lies in a neighborhood of b so that $u(r)$ never drops below a for any r. Consider $u(0) > b$ so that $du/dr = v$ initially becomes negative. Then, $u(r)$ starts vertically downward and bends to the left, bending more than the level curve to which it is initially tangent, since the representative point must run "downhill." $u(r)$ oscillates about b, approaching b as $r \to \infty$. Thus there appears to exist a whole sequence of solutions for which $(du/dr)|_R = 0$, each corresponding to a different number of nodes in the domain $(0, R)$. The existence of such oscillatory solutions in the domain $(0, \infty)$ can be established rigorously (see Appendix B). We shall see later that it is these oscillatory solutions which bifurcate from the radially uniform solutions along the break-back portion of the I-V characteristic.

b. $(du/dr)|_R < 0$. It is clear that for the oscillatory solutions described above, du/dr oscillates between certain fixed limits; in fact, since $dA/dr < 0$, the minimum value attained by du/dr increases with every extra node the solution possesses, so that as du/dr is required to become more and more negative at R, fewer and fewer of these oscillatory solutions can satisfy the boundary condition. For $(du/dr)|_R$ sufficiently negative [or $u(R) < a$] these oscillatory solutions are never able to satisfy the boundary conditions so that they cease to exist and we are left with only three solutions, one starting to the left of a, one starting between b and c, and another starting just below c. These last three solutions exist for any radial boundary conditions corresponding to non-negative heat loss at $r = R$. For all three of these solutions, $du/dr \leq 0$ for all r.

Consider now $\lambda' < \lambda_1$. Figure 10 consists of a sketch in the phase plane of lines of constant A for a value of λ in this range. a' is the point of intersection of the line $\lambda = \lambda'$ with the set of solution points to Eq. (36) [see Fig. 9(a)]. Here we see that only one solution may exist for any given boundary condition. For $u(0) = a'$, $u(r)$ is a constant. For $u(0) < a'$, $du/dr < 0$ for all r, and for $u(0) > a'$, $du/dr > 0$ so that $u(r)$ increases monotonically. Therefore, for a given $\lambda = \lambda' < \lambda_1$, only one solution can exist which satisfies a given boundary condition at $r = R$. Similar considerations show that the same holds true for $\lambda > \lambda_2$.

Therefore, multiple solutions to (30) can exist only for $\lambda \in (\lambda_1, \lambda_2)$. For λ outside that range, (32) possesses a unique solution (see Fig. 11).

In this way, certain general features of solutions to the system (23)–(25) begin to emerge. Multiple solutions may exist only for $E = E'$ such that the left-hand side of (9) is less than zero (negative differential resistance). For $du/dr|_R = 0$, the number of solutions which can exist in this range depends upon the value of R; the greater the value of R is, the greater the number of possible solutions. But if we impose boundary conditions which require

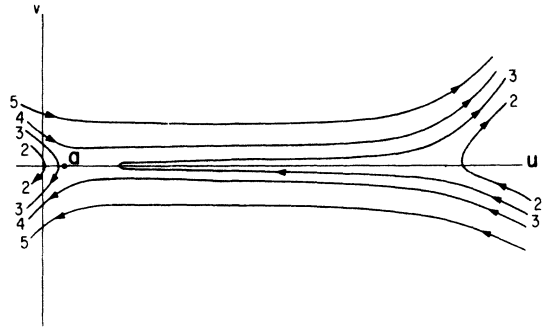

FIG. 10. Constant A level curves in the phase plane for $\lambda = \lambda' < \lambda_1$ [see Fig. 9(a)]. Values of A in arbitrary units.

that $T(R) < T'$, where T' is the smallest of the three solutions of (8) for a given E', we saw that only three corresponding solutions of Eqs. (23) and (25) can exist. In general, the greater the amount of radial heat loss we permit, the fewer the number of solutions which can exist. We now seek to establish analytically the existence of solutions to Eqs. (23)–(25) corresponding to radially dependent temperature and current distributions.

2. *Bifurcation analysis*

In Appendix C we establish criteria for the existence of bifurcation points on the I-V characteristic determined by solutions of (8).[63] At these points, solutions of Eqs. (23)–(25) corresponding to radially dependent temperature distributions split off from the radially uniform solution as E passes through a critical value E^*.

It is shown that bifurcation points can occur only along the segment of the characteristic for which $dI/dV < 0$, and that a sequence of these points exists, starting just above the turnaround point. The nth bifurcation point is characterized by a wave number, k_n, the determination of which is discussed below (see Fig. 23).

The location of the bifurcation points is determined from the eigenvalue problem obtained by linearizing Eqs. (23)–(25) about a radially uniform solution. In general, it is found that these new solutions may be expanded about their respective bifurcation points as Taylor series in an amplitude parameter, ϵ:

$$T(r, \epsilon) = T + \epsilon T'(r) + \tfrac{1}{2}E^2 T''(r) + \cdots,$$
$$E(\epsilon) = E + \epsilon E' + \tfrac{1}{2}\epsilon^2 E'' + \cdots. \tag{37}$$

The first term on the right-hand side is the value of the radially uniform solution at the bifurcation point. Successive terms in the expansion may be determined, and the properties of the solution established in a neighborhood of the bifurcation point.[64–66]

It is particularly instructive to look at the first-order terms in the expansion. It is found that for the solution bifurcating at k_n (Fig. 23),

$$T_n'(r) = \phi_0(k_n r) - \frac{(2 + E/E_0)\sigma(T, E)E}{k_n^2 K} E_n', \tag{38}$$

$$E_n' = -E^2 \frac{\partial^2\sigma}{\partial T^2}\int_0^R r\,dr\,\phi_0^3(k_n r)\left(2\frac{\partial\sigma}{\partial T}\left(2 + \frac{E}{E_0}\right)\right.$$
$$\left.\times\left\{1 - \left[\frac{\partial^2\sigma}{\partial T^2}\Big/\left(\frac{\partial\sigma}{\partial T}\right)^2\right]\left(\sigma\frac{\partial\sigma}{\partial T}E^2/k_n^2 K\right)\right\}\right)^{-1}, \tag{39}$$

and

$$I_n' = \pi R^2\sigma(T, E)\left(1 + \frac{E}{E_0}\right)$$
$$\times\left[1 - \frac{2 + E/E_0}{1 + E/E_0}\left(\frac{\partial\sigma}{\partial T}E^2/k_n^2 K\right)\right]E_n', \tag{40}$$

where I_n' is the first-order term in the expansion of the total current. All the coefficients on the right-hand side of Eqs. (38)–(40) are to be evaluated at the nth bifurcation point. $\phi_0(k_n r)$ is the zero-order Bessel function normalized on the interval $(0, R)$ where k_n is determined by the boundary condition $(dT/dr)|_R = 0$, so that $J_1(k_n R) = 0$.

For the solution bifurcating at k_1, T_1 decreases monotonically in the domain $(0, R)$. The solution breaking off at k_2 contains one node and, in general, the solution bifurcating at the point determined by k_n possesses $n-1$ nodes. It is clear that while the solutions bifurcating for $k_n > k_1$ do satisfy the system (23)–(25), they are not really of

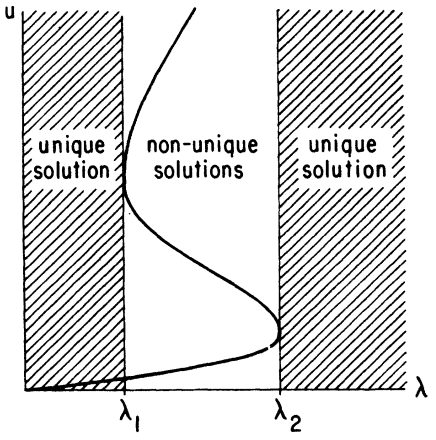

FIG. 11. Sketch in $u-\lambda$ plane indicating regions in which Eq. (32) possesses a unique solution. Solid curve is graph of solutions $u(\lambda)$ of Eq. (36).

physical interest because the existence of nodes in the radial temperature distribution causes them always to be unstable (see Sec. VI). We shall therefore concern ourselves here only with the properties of the solution bifurcating at k_1 which, for $\epsilon > 0$, has a temperature peak at $r = 0$. Several general statements can be made concerning the sign of E_1' and I_1' in this case. In (39) we note that

$$\int_0^R r\,dr\,\phi_0^3(k_1 r) = \tfrac{4}{3}\int_0^R r\,dr\,\phi_1^3(k_1 r) > 0,$$

since $\phi_1(k_1 r) > 0$ for $r \in (0, R)$, so that the sign of E_1' is determined by that of the term

$$1 - \left[\frac{\partial^2\sigma}{\partial T^2}\Big/\left(\frac{\partial\sigma}{\partial T}\right)^2\right]\left(\sigma\,\frac{\partial\sigma}{\partial T}E^2\Big/k_1^2 K\right).$$

$Kk_1^2 = (\partial\sigma/\partial T)E^2 - \alpha > 0$, so that the ratio $(\partial\sigma/\partial T)E^2/Kk_1^2 > 1$. Therefore, if $(\partial^2\sigma/\partial T^2)\sigma/(\partial\sigma/\partial T)^2 \geq 1$ at the bifurcation point, E_1' is *always* greater than zero, regardless of the exact location of the bifurcation point. This is true, for example, for $\sigma = \sigma_0 e^{\beta T}$. For $\sigma(T)$ increasing more slowly than this, e.g., for $\sigma = \sigma_0 e^{-C/T}$, the ratio $(\partial^2\sigma/\partial T^2)\sigma/(\partial\sigma/\partial T)^2 < 1$, so that no general statement may be made concerning the sign of E_1'. Looking now at I_1', we see the coefficient of $(\partial\sigma/\partial T)E^2/Kk_1^2$ is greater than 1 so that I_1' always has a sign opposite to that of E_1'.

It should be pointed out that two solutions branch off at each bifurcation point, one corresponding to $\epsilon > 0$, the other to $\epsilon < 0$. For the choice $\epsilon > 0$, we see that the solution bifurcating at k_1 decreases monotonically as r increases. Along the branch of the characteristic bifurcating at k_1, determined with $\epsilon > 0$, solutions all have temperature maximums at $r = 0$.[67] We are interested in this branch of the characteristic and, in the following analysis, shall always consider $\epsilon > 0$.

In Table III the first three terms in the expansions

$$I_1(\epsilon) = I_1 + \epsilon I_1' + \frac{\epsilon^2}{2} I_1'' + \cdots,$$

$$E_1(\epsilon) = E_1 + \epsilon E_1' + \frac{\epsilon^2}{2} E_1'' + \cdots$$

are evaluated for various device radii, with $d = 1\ \mu$. The data were obtained using material parameters $K = 4\times10^{-3}$ W/cm °K, $E_0 = 3.7\times10^4$ V/cm, and $\sigma(T)$ given in Fig. 2. Turnaround voltage for this set of parameters is 15.8 V, and current density at turnaround is 3.86×10^2 A/cm^2 (see Fig. 13).

Several interesting features concerning the dependence of $I_1(\epsilon)$ and $E_1(\epsilon)$ on device dimensions R and d can be determined. From Table III we see that for normal device geometries in which $d/R \ll 1$, the first bifurcation point lies very near the voltage turnaround. As d/R increases, the bifurcation point begins to move away from the voltage turnaround. This effect first becomes appreciable for $R = 2$ or $3d$. Here, the boundary condition of no heat loss to the sides becomes inaccurate; taking lateral heat loss into account probably accentuates this trend. In all cases listed, $E_1' > 0$, so that the new branch of the I-V characteristic lies right along the radially uniform branch, at least initially (see Fig. 12). If $R \gg d$, both I_1' and I_1'' are less than zero, so that to second order, the new branch of the I-V characteristic continues to drop toward lower current. But for $R \gtrsim 2$ or $3d$, $E_1'' < 0$ and $I_1'' > 0$ so that the branch of the I-V characteristic corresponding to this solution would eventually begin rising as E drops (see Fig. 12). This is to be expected; as we shall see later, for the radially dependent solution at a given $E = E^0$, the hot region in the device interior extends over a relatively small range, on the order of a few microns. Outside this region, the temperature is low, being essentially equal to the lowest temperature solution of (8) obtained using the same value of $E = E^0$. [This solution of (8), in fact, determines the low-current branch of the radially uniform I-V characteristic as E^0 varies between zero and E_1, the turnaround field.] Therefore, for R very large, the hot region will have a negligible effect upon the current that the device is able to carry. But as R decreases, the hot region becomes more and more important, until finally, a large percentage of the total device current flows through this region, even

TABLE III. Values of coefficients in the expansion of the current density $j(\epsilon)$ and electric field $E(\epsilon)$ about the lowest bifurcation point for model B as a function of device radius for constant thickness $d = 1\mu m$. $K_l = 4$ mW/cm °K, and $E_0 = 3.7\times10^4$ V/cm. Thus, $j(\epsilon) = j_B + \epsilon j_B' + \frac{1}{2}\epsilon^2 j_B'' + \cdots$, $E(\epsilon) = E_B + \epsilon E_B' + \frac{1}{2}\epsilon^2 E_B'' + \cdots$.

R (μ)	j_1 (A/cm^2)	E_1 (V/cm)	T_B	j_B (A/cm^2)	j_B' (A/cm^2)	j_B'' (A/cm^2)	E_B (V/cm)	E_B' (V/cm)	E_B'' (V/cm)
1000	3.867×10^2	1.5794×10^5	19.0899	3.8677×10^2	-1.253×10^2	-3.399×10^7	1.5794×10^5	1.498×10^{-2}	-1.04066×10^4
100	3.867×10^2	1.5794×10^5	19.0938	3.8685×10^2	-1.253×10^3	-3.397×10^7	1.5794×10^5	1.498×10^1	-1.0407×10^6
10	3.867×10^2	1.5794×10^5	19.4898	3.9489×10^2	-1.283×10^4	-3.2165×10^7	1.5794×10^5	1.498×10^4	-1.0444×10^8
6	3.867×10^2	1.5794×10^5	20.206	4.0948×10^2	-2.229×10^4	-2.865×10^7	1.57905×10^5	6.935×10^4	-2.9188×10^8
3	3.867×10^2	1.5794×10^5	23.656	4.809×10^2	-5.364×10^4	-7.1087×10^6	1.574×10^5	5.544×10^5	-1.19699×10^9
1	3.867×10^2	1.5794×10^5	75.18	1.843×10^3	-8.2616×10^5	1.1915×10^9	1.305×10^5	1.458×10^5	-1.023×10^{10}

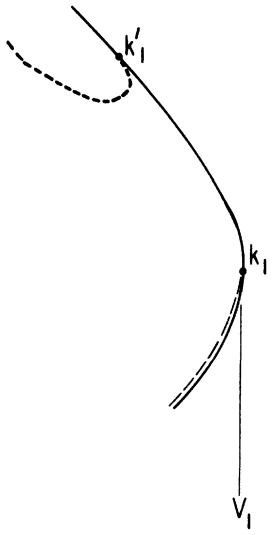

FIG. 12. Schematic in I-V plane indicating location of first bifurcation point and behavior of branch determined by radially dependent solutions ($\epsilon > 0$) for (1) $k = k_1$, $R \gg d$, and (2) $k = k_1'$, $R \approx 2d$.

when it is quite small, and the device resistance is substantially reduced due to its presence.

Finally, we reiterate that if σ is only weakly dependent on T, we have $E_1' < 0$ and $I_1' > 0$ for R small enough. In general, the weaker the dependence of σ on T, the larger the value of R for which this is true.

Unfortunately, the expansion technique used in Appendix C yields information concerning the radially nonuniform solutions only in a neighborhood of the bifurcation points. In order to determine the behavior of these solutions at general voltages and currents, it is necessary to resort to numerical techniques.

3. *Numerical results*

In Fig. 13, the branch of the I-V characteristic which bifurcates at k_1 for $\epsilon > 0$ is graphed along with the previously determined radially uniform branch. These results were obtained by direct numerical solution of Eqs. (23)–(25) on a lattice of 100 mesh points using the same material parameters as above (see Table III). We used $d = 1\ \mu$, $R = 10\ \mu$, and $(du/dr)|_R = 0$ for the boundary conditions.

The portion of the I-V characteristic associated with the radially dependent solutions lies just above the radially uniform branch until approximately 2 V. Then it rises almost vertically. Temperature profiles at points A through E are given in Fig. 14.

We see that the temperature profiles of the solutions along this new branch of the characteristic show a very pronounced peak at $r = 0$. Looking at the temperature distribution as V decreases from the bifurcation point to about 2 V, we see that the value of T at $r = 0$ continues to increase rapidly. No real "channel" is yet defined, and the temperature drops exponentially from $r = 0$. But once T ($r = 0$) reaches approximately 700 °K, the hot central region begins to broaden, a well-defined hot channel forms, and the second branch of the I-V characteristic pulls away from the first. The temperature is now approximately constant in the hot region. In the vertical portion of the I-V characteristic, the only change in the solution is the broadening of the hot channel as I is increased. As mentioned in Sec. IV, the temperature in the channel is approximately 700 °K, the temperature at which $\sigma(T)$ begins to saturate.

For a wider device of the same thickness, we would expect the I-V characteristic to be essentially the same. But for substantially narrower devices we expect the branch determined by radially dependent solutions of Eqs. (23)–(25) to bend upward at higher voltages because a larger percentage of the total device current flows through the small hot region.

To investigate the validity of this last assertion, we solved Eqs. (23)–(25) numerically, with $V = 12$ V and $d = 1\ \mu$, for various device radii. The ma-

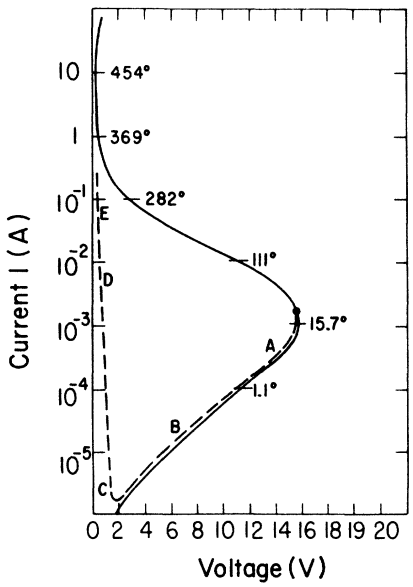

FIG. 13. Current-voltage characteristic obtained by numerical solution of the system (23)–(25). Solid curve: radially uniform branch; dashed curve: branch arising from channelized current flow. $d = 1\ \mu$m, $R = 10\ \mu$m, $K_I = 4$ mW/cm °K, $E_0 = 3.7 \times 10^4$ V/cm, and $L = 2.45 \times 10^{-8}$ WΩ/°K. Temperatures listed are °K above ambient $T_0 = 295$ °K.

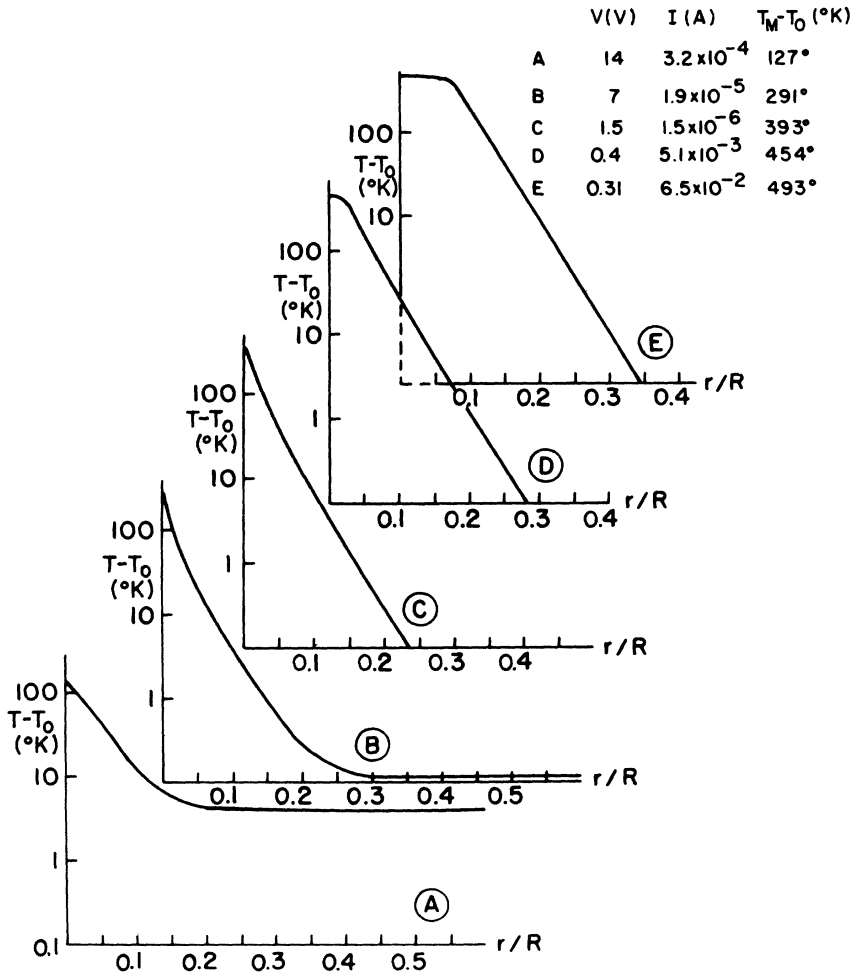

FIG. 14. Radial temperature profiles at points A through E of characteristic in Fig. 13. R is the device radius, $T_M - T_0$ is the maximum temperature in channel above ambient, and $T_0 = 295$ °K.

terial parameters in this calculation were the same as used previously for model B. The results of the calculation are presented in Table IV. The current densities listed correspond to radially dependent temperature profiles. The current density at this voltage on the radially uniform I-V characteristic is $J_n = 4.1\times10^1$ A/cm^2 (see Fig. 13). We see that for $R = 10$ μ the current density, determined by the radially dependent solution of Eqs. (23)–(25), is only about 3% greater than J_n. But for $R = 1.6$ μ, the current density is already almost five times greater than J_n. In devices less than about 8 or 10 μ in diameter (when $d = 1$ μ), the I-V characteristic determined by radially dependent solutions of Eqs. (23)–(25) lies at substantially higher current densities for essentially all voltages.

4. *Effect of radial boundary conditions*

Finally, we discuss the effect of radial heat loss upon the various branches of the I-V characteristic. For devices of very large radii, the effect of moderate radial heat loss is quite negligible since the radial heat flow at the outer radius will depress the temperature profile only near the boundary. But as R decreases, the effect becomes more substantial, and we should expect average current densities determined by solutions of Eqs. (23)–(25) to decrease for constant V as $(dT/dr)|_R$ becomes more negative. We found this to be true, but the effect is really very small even for devices of 10-μ radius and very high-temperature gradients at $r = R$.

For $V = 14$ V, the radially dependent solution of Eqs. (23)–(25) lies at $I = 3.177\times10^{-4}$ A for no heat-flow boundary conditions when $R = 10$, $d = 1$ μ. On the radially uniform branch, I is about two percent less. For $(dT/dr)|_R = 3.8\times10^4$ °K/cm, the corresponding solutions lie at 3.149×10^{-4} and 2.869×10^{-4} A. The two branches lie at slightly lower currents and are a bit more separated.

For $T(R)$ locked at ambient, the phase-plane analysis performed at the beginning of this section indicates that at most three solutions can exist for

TABLE IV. Average current density on the branch of characteristic determined by radially dependent solutions (branch c, Fig. 17) as a function of device radius R for $V=12$ volts using model B. Current density on radially uniform branch (branch a, Fig. 17) at this voltage is 4.1×10^{1} A/cm^2. $d=1$ μm, $K_l=4$mW/cm °K, $E_0=3.7\times10^{4}$ V/cm.

R (cm)	Current Density (A/cm^2)
10^{-3}	4.256×10^{1}
8×10^{-4}	4.458×10^{1}
6×10^{-4}	4.884×10^{1}
4×10^{-4}	6.029×10^{1}
3×10^{-4}	7.56×10^{1}
2×10^{-4}	1.236×10^{2}
1.75×10^{-4}	1.556×10^{2}
1.6×10^{-4}	1.896×10^{2}

a given V. Temperature profiles of these three solutions, and the I-V characteristic determined by them are illustrated in Fig. 15. The branch of the I-V characteristic which has disappeared corresponds to solutions which describe orbits about point b in Fig. 9(b). Again for the relevant material parameters and $R\gtrsim10d$, we expect the two low-current segments of the I-V characteristic to lie close together for a range of voltages below turnaround.

B. Model A

Unfortunately, for the problem described by model A, none of the simple techniques used to investigate general solutions of Eqs. (23)–(25) apply. Also, the use of numerical techniques becomes impractical. The large gradients involved in both the temperature and field for solutions at high-current densities would require a prohibitive number of mesh points in two dimensions.

Although it appears difficult to determine analytically the properties of solutions of Eqs. (26)–(31) for general I and V, it is still possible to prove the existence of additional branches of the I-V characteristic. As with model B, it is possible to prove that solutions corresponding to radially dependent temperature and current distributions bifurcate from points along the breakback portion of the I-V characteristic determined by radially independent solutions of Eqs. (26)–(31).

In Appendix D we establish criteria for the existence of such bifurcation points. The analysis is essentially the same as it was with model B. The temperature and current density can be expanded about the bifurcation points as Taylor series in an amplitude parameter ϵ. Successive coefficients in the series may be evaluated and properties of these new solutions determined.

The results of these calculations are essentially the same as those presented above for model B. When $R\gg d$, the first bifurcation point lies very near the voltage turnaround point. Two solutions bifurcate at this point, one for positive and one for negative ϵ. The branch for $\epsilon>0$ corresponds to solutions which possess a temperature maximum at $r=z=0$. As with model B, these are the solutions of interest to us. The solution bifurcating from the lowest critical point is a monotonic function of r and z, and, in general, the solutions bifurcating at higher currents possess nodes in both the r and z direction.

For the branch of the I-V characteristic determined by the solution bifurcating at the first critical point, we again obtain $I'<0$ and $V'>0$ for normal device geometries, so that the branch determined by $\epsilon>0$ follows along the lower branch of the I-V characteristic determined by radially uniform solutions of Eqs. (26)–(31).

Table V presents results relating the current at turnaround voltage to current at the first bifurcation point as a function of device thickness d for constant device radius $R=10$ μ. Also included are our results for the first-order change in current, I', and the first-order change in voltage, V', for the solution bifurcating at this point. These results were obtained using $E_0=2.5\times10^{4}$ V/cm and $K_l=2.2$ mW/cm °K.

The close analogy of the results of this calcula-

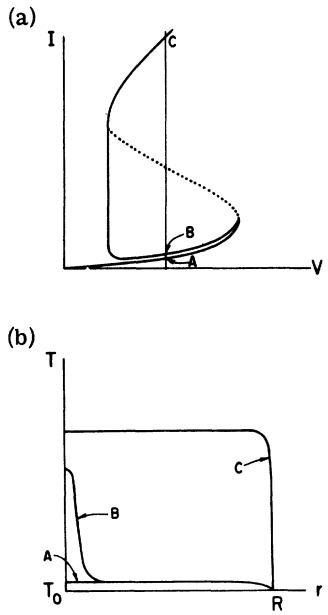

FIG. 15. Schematic of (a) I-V characteristic (solid line) and (b) radial temperature profiles at points A, B, and C of (a) for device geometry in which $R\gg d$ and $T(R)=T_0$, ambient. R is the device radius.

TABLE V. Values of coefficients in expansion of current $I(\epsilon)$ and voltage $V(\epsilon)$ about the lowest bifurcation point in model A as a function of device thickness for constant $R = 10\ \mu$m. $K_I = 2.2$ mW/cm °K, $E_0 = 2.5 \times 10^4$ V/cm, electrodes locked at ambient. $V(\epsilon) = V_{B1} + \epsilon V'_{B1} + \cdots$, $I(\epsilon) = I_{B1} + \epsilon I'_{B1} + \cdots$.

$d(\mu)$	V_1 (V)	I_1 (A)	V_{B1} (V)	I_{B1} (A)	V'_{B1} (V)	I'_{B1} (A)
0.25	4.222	1.54×10^{-2}	4.222	1.54×10^{-2}	0	-1.88×10^{-5}
0.5	7.137	4.56×10^{-3}	7.137	4.58×10^{-3}	3.7×10^{-6}	-6.05×10^{-6}
1.0	11.78	1.38×10^{-3}	11.78	1.41×10^{-3}	3.6×10^{-5}	-1.65×10^{-6}
5.0	33.26	1.00×10^{-3}	33.16	1.42×10^{-3}	4.3×10^{-3}	-2.79×10^{-7}
10.0	48.32	4.00×10^{-5}	44.82	1.05×10^{-4}	2.8×10^{-1}	-2.76×10^{-6}

tion with those obtained using model B makes us think that the general behavior of the branch of the I-V characteristic determined by the solutions which bifurcate from the first critical point is essentially the same for both model systems. For $R \gg d$, this branch lies right along the low-current branch determined by radially uniform solutions of Eqs. (26)–(31) until voltages on the order of 1 V.[68] At this point the central temperature in the hot region is approximately 700 °K for $Ge_{15}Te_{81}X_4$. The I-V characteristic here turns essentially vertical, and the central hot region begins to expand in diameter. The temperature distributions both inside and outside this hot region are relatively flat, and in the transition region the temperature drops exponentially between its two limits. For $R \gtrsim d$, this branch begins to rise at much higher voltages, so that when $R \approx 2d$ the segment of the I-V characteristic determined by radially dependent solutions never does lie close to the low-current radially uniform branch of the characteristic.

VI. TEMPORAL STABILITY OF STEADY-STATE SOLUTIONS

In this section we consider the temporal stability of the various solutions to Eqs. (23)–(25) and (26)–(31) discussed in Sec. V. In particular, we shall consider the stability of these solutions with respect to perturbations which keep the total current through the device constant. This corresponds to the physical situation of an infinite load resistance and is the most stable circuit configuration. We do not consider the effects of additional circuit capacitances and inductances, but deal only with the ideal situation of a system completely defined by Eqs. (1)–(3) with appropriate boundary conditions. The effects of various capacitances and inductances on a device's stability in a given operating situation have been discussed elsewhere.[69,70]

In Appendix E a local stability analysis is performed for both the radially uniform solutions discussed in Sec. IV and the radially dependent solutions derived in Appendices C and D. It is found that for both models A and B, the radially uniform branch of the I-V characteristic is unstable above the first bifurcation point. It is also found that all solutions bifurcating from the higher critical points are unstable.

It is shown, in general, that the answer to the question of stability of a given solution parameterized in ϵ about some bifurcation point is determined by the sign of

$$\omega(\epsilon) = \omega_0 + \epsilon\omega' + \tfrac{1}{2}\epsilon^2\omega'' + \cdots .$$

If $\omega > 0$, the solution is unstable, and if $\omega < 0$, the solution is stable. For all solutions bifurcating at critical points other than the first, $\omega_0 > 0$, so that $\omega(\epsilon) > 0$. For the solution bifurcating at the first critical point, though, $\omega_0 = 0$, so that it is required to go to first order in ϵ to determine the stability of this branch of the I-V characteristic for $|\epsilon| \ll 1$.

We first recall that we are interested in the question of stability of the branch bifurcating from k_1 corresponding to solutions which possess a temperature maximum in the device interior. This we saw corresponds to the choice $\epsilon > 0$.

For model B, it is shown in Appendix E that

$$\omega'_1 = \left\{ \frac{\partial^2\sigma}{\partial T^2} E^2 \int_0^R \phi_0^3(k_1 r) r\,dr + \left(2 + \frac{E}{E_0}\right) E \frac{\partial\sigma}{\partial T}\left[1 - \left(\frac{\partial^2\sigma}{\partial T^2}\Big/\frac{\partial\sigma}{\partial T}\right)\frac{\sigma E^2}{k_1^2 K}\right] E' \right\} \times \left[C + \frac{4\pi\mu}{c}\frac{\partial\sigma}{\partial T}\left(2 + \frac{E}{E_0}\right)\frac{\sigma E^2}{k_1^2 K}\right]^{-1}, \tag{41}$$

where all the coefficients on the right-hand side are evaluated at the first bifurcation point. From Eq. (C15),

$$2\frac{\partial\sigma}{\partial T}\left(2 + \frac{E}{E_0}\right)\left\{1 - \left[\frac{\partial^2\sigma}{\partial T^2}\Big/\left(\frac{\partial\sigma}{\partial T}\right)^2\right]\left(\frac{\partial\sigma}{\partial T}\sigma E^2\Big/k^2 K\right)\right\} E' + \frac{\partial^2\sigma}{\partial T^2} E \int_0^R r\,dr\,\phi_0^3(kr) = 0 . \tag{42}$$

Since $\int_0^R r\,dr\,\phi_0^3(kr) = \frac{4}{3}\int_0^R \phi_1^3(kr) r\,dr > 0$ for $k = k_1$, we see that the first term on the left-hand side of (42) is less than zero. Using this fact, it is clear from Eq. (41) that ω'_1 is greater than zero for any $\sigma(T)$ and E. Therefore, the solution bifurcating at

k_1 with $\epsilon > 0$ is unstable in a neighborhood of the critical point. Calculation shows the same result to be true for the solutions determined in model A.

Finally, for model B we investigated numerically the temporal stability of the remainder of the branch of the I-V characteristic bifurcating at k_1 with $\epsilon > 0$. Solutions on this branch have $dT/dr < 0$, $r \in (0, R)$ (see Fig. 13). In the calculation we again required that the total current through the device remain constant. It was found that this branch of the I-V characteristic was stable on its vertical segment for currents greater than approximately 2×10^{-4} A for a device 20 μ in diameter, 1 μ thick, and $E_0 = 3.7 \times 10^4$ V/cm, $K_l = 4$ mW/cm °K. These are the same material parameters used in calculating the I-V characteristic illustrated in Fig. 13. The use of a finite load resistance would move the point of instability to slightly higher currents. In general, the smaller the load resistance, the higher the current at which the instability would appear.

The stability of the relevant branches of the I-V characteristic is summarized in Fig. 16. The dashed-line segments are unstable and the solid-line segments are stable. For the dotted portion at high currents, we have not determined the stability of the solutions.

VII. DISCUSSION AND CONCLUSION

The primary results of the above analysis are reviewed using Fig. 17. We have seen, in general, that the existence of a region of negative differential resistance on the I-V characteristic determined by radially uniform solutions of the thermal balance equation implies, under certain circumstances, the existence of multiple branches of the I-V characteristic. These new branches bifurcate from the break-back portion

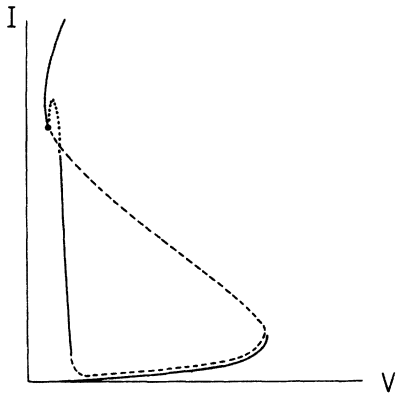

FIG. 16. Stability of relevant branches of I-V curve for very large load resistances. Solid curve: stable; dashed curve: unstable: dotted curve: stability not determined.

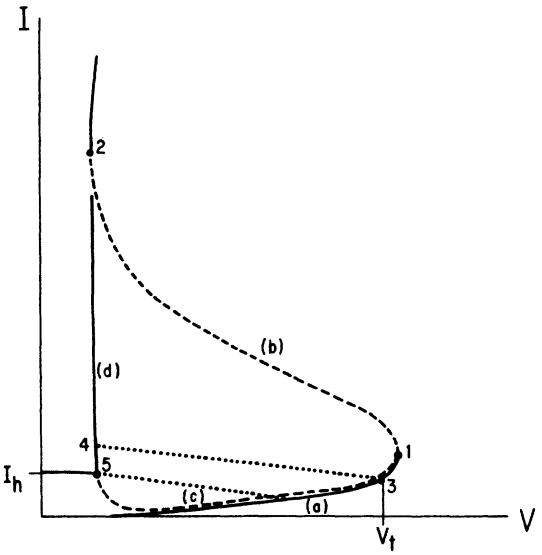

FIG. 17. Predicted current-voltage characteristic for $R \gg d$. Solid curve: stable; dashed curve: unstable; dotted curve: load line.

(segment b) of the characteristic and were seen to correspond to temperature and current distributions which possess various numbers of nodes in the radial and axial directions. One of these, bifurcating nearest the turnaround point, is determined by solutions for which the temperature is sharply peaked at the device center. We found that for device geometries in which $R \gtrsim 5d$, this branch, denoted by c in Fig. 17, initially lies very near the low-current segment of the characteristic a when values for K and σ appropriate to the chalcogenide glasses, are used. For voltages lower than 1 or 2 V, this is no longer true, and the characteristic turns nearly vertical d. Along this portion the current flow takes place predominantly in a high-temperature filament or channel in which the temperature distribution is nearly flat. Outside of this region, the temperature drops exponentially to values near ambient. The temperature in the conducting channel was determined to lie very near values at which $\partial^2\sigma/\partial T^2$ turns negative. (For $Ge_{15}Te_{81}X_4$ this is approximately 700–750 °K.)

Finally, it was shown that the dashed portion of segments b and c are locally unstable against temperature and field perturbations which keep the total current through the device constant, and that branches a and d are stable with respect to such perturbations.

The above results were obtained by analyzing the MET theory in a specific device configuration for a particular set of material parameters relevant to the chalcogenide glasses. In general, the specific form of the I-V characteristic pre-

dicted by the MET theory depends upon the device geometry and heat-flow boundary conditions, as well as the dependence of σ and K on the temperature and field.

We have seen that for device geometries in which $R \gg d$ and the electrodes provide strong thermal coupling to a heat sink, branches a and c (Fig. 17) of the group-I-V characteristic lie very close together for V greater than 1 or 2 V, regardless of the radial boundary conditions for the temperature. The separation between these branches increases if (i) R is decreased until it is only slightly greater than d, or (ii) the extent of the longitudinal coupling to a heat sink is reduced. In fact, when device heat loss is primarily in the radial direction, we expect branch c not to fall to lower currents at all, but have I increase as V decreases over its entire length. The limiting behavior in this case is reached when all the heat flow is in the radial direction so that (26) becomes

$$\frac{1}{r}\frac{d}{dr}\left(rK\frac{dT}{dr}\right)+j_z E_z = 0 . \tag{43}$$

For the system described by Eq. (43) it is possible to prove that the I-V characteristic is unique as a function of I.

Finally, we note that the stronger the dependence of σ on temperature, the more sharply defined the conducting channel. If σ were only a weak function of T, the central heat region would be relatively broad and ill defined.[71] Also, the weaker the dependence of σ on temperature, the larger the separation between branches a and c of the characteristic for a given ratio of d/R and set of thermal boundary conditions.

The particular form of the characteristic sketched in Fig. 17 is critically dependent on the field dependence of σ, the rapid increase and subsequent saturation of σ with increasing temperature, the enhancement of K at high temperatures, and the thin film geometry in which $R \gg d$ and the electrodes provide very strong coupling to a heat sink.

A. Comparison with previous results

It has been known for quite some time that a wide variety of mechanisms capable of inducing negative differential resistance behavior in a material can cause the formation of high-current filaments (S-shaped I-V curve) or high-field domains (N-shaped I-V characteristic). Perhaps the best-known example of the latter is the Gunn effect.[72] As mentioned previously, the possibility of thermally induced negative differential conductivity causing such behavior was noted as early as 1936 by Spenke and co-workers.[55-57] In that work the equation

$$K\frac{d^2\Theta}{dx^2}-\Theta(x)+(1+\Theta^2)u^2=0,$$

$$x\in(-X,X),\quad \left.\frac{d\Theta}{dx}\right|_{\pm X}=0,$$

where u is a constant parameter, was solved by quadratures in terms of elliptic integrals. It was found that a series of solutions exist and that the I-u characteristic obtained by solution of this equation possessed several branches (Fig. 18). It was also noted that if either K were decreased or X made larger, these branches could "bend down" to lower currents after bifurcating from the x-independent solution (Fig. 18).

In that series of papers it was also shown that the linearized forms of the more general equations

$$K\frac{d^2\Theta}{dx^2}-\Theta(x)+f^{-1}(\Theta)u^2=0,\quad \left.\frac{d\Theta}{dx}\right|_{\pm X}=0$$

and

$$\frac{K}{r}\frac{\partial}{\partial r}\left(r\frac{\partial\Theta}{\partial r}\right)+\frac{K}{r^2}\frac{\partial^2\Theta}{\partial\theta^2}-\Theta(r,\theta)+f^{-1}(\Theta)u^2=0,$$

$$0\le r<R,\quad 0\le\Theta<2\pi,\quad \left.\frac{\partial\Theta}{\partial r}\right|_R=0$$

possess solutions when $dI/du<0$ on the curve defined by solutions of[73]

$$-\Theta+f^{-1}(\Theta)u^2=0 .$$

A recent paper by Landauer and Woo[74] presents a discussion of the results obtained by Spenke *et al.*

Much more recently, Croitoru, and co-workers investigated numerically the solutions of Eq. (23) for $K=\text{const}$, $\sigma(T)=\sigma_0 e^{\beta T}$, and the boundary condition $(dT/dr)|_R=0$.[23,24] They found that more than one branch of the characteristic can exist, but obtained the result that the branch corresponding to concentrated current flow does not break back along the radially uniform characteristic after bifurcation. This apparently disagrees with our results. We have found that for $\sigma(T)=\sigma_0 e^{\beta T}$, it can be shown that even when σ is independent of E, the branch bifurcating nearest the voltage turnaround drops to lower currents initially, regardless of the ratio d/R (see Appendix C). A possible explanation of this difference is that an insufficient number of mesh points were used by Croitoru and Popescu in obtaining the radially dependent solutions, so that the rapid drop in temperature was not resolved sufficiently, resulting in an overestimate on their part of the total current for a given solution.

Shousha has also investigated numerically solutions of the equation

$$\frac{K}{r}\frac{d}{dr}\left(r\frac{dT}{dr}\right)-\frac{\lambda}{d}(T-T_0)+\sigma E^2=0,$$

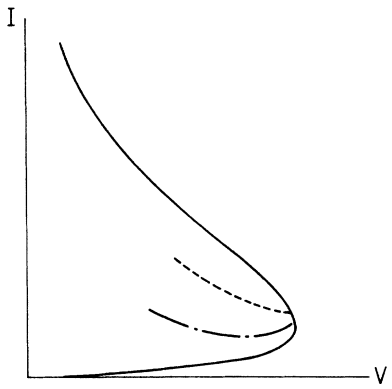

FIG. 18. Current-voltage characteristic obtained by Spenke as solution of $K(d^2\theta/dx^2) - \theta(x) + (1-\theta^2)u^2 = 0$. Solid curve: x-independent branch; dash-dotted curve: behavior of branch bifurcating at first critical point for $K = 0.00403$; dashed curve: behavior of branch bifurcating at first critical point for $K = 0.0385$ (fixed X) [Spenke (Ref. 55)].

with the boundary condition $T(R) = T_0$.[27] He used $\sigma(T, E) = \sigma_0 e^{(-C/T)+E/E_0}$, $R = 5\times10^{-3}$ cm, and $d = 5\times10^{-5}$ cm. In his calculation a value of λ/d was used which is substantially smaller than the value of $8K/d^2$ we found appropriate for this coefficient (Fig. 8). Consequently, the portion of the characteristic designated by c in Fig. 17 does not lie as close to branch a in his calculation. But for the choice of $\lambda = 5\times10^{-1}$ W/cm^2 °K and $K = 5\times10^{-3}$ W/cm °K he does find that this segment drops to lower currents near turnaround. Also, because the $\sigma(T)$ used in his calculations did not possess the rapid anomalous increase and subsequent saturation behavior exhibited in Fig. 2, the segment of the characteristic corresponding to constricted current flow did not exhibit the behavior summarized by branch d of Fig. 17.

Preliminary results obtained by numerical solution of the equation

$$\frac{d^2T}{dz^2} - \frac{\lambda}{dK}(T - T_0) + \frac{\sigma E^2}{K} = 0$$

for the boundary condition $T(R) = T_0$ were also presented in a recent paper by Thomas and Male.[14] They again found the existence of solutions corresponding to channelized current flow, but had not yet determined the full I-V characteristic.

Finally, Kaplan and Adler[25] have recently attempted to obtain numerically solutions to the thermal balance equation in three dimensions. They required conservation of current and specified the temperature on the device boundary. The geometry used was that of a cylinder much larger in radius than height and they chose material parameters appropriate to the chalcogenide glasses. Also, they assumed that the current flowed only in the axial direction. With these assumptions, they obtained solutions for two model systems: (i) the standard thermal model (STM) in which $\sigma = \sigma(T, E)$ and (ii) the virtual electrode model (VEM) in which no field dependence of the conductivity is assumed, but the electrical boundary conditions are modified by a parallel displacement of each of the equipotential planes of the electrodes by a small distance, Δ, into the material. The voltage drop is then constrained to be entirely in the region between the two equipotential planes. This was done in an attempt to approximate tunneling and space-charge injection at the electrodes. In both these cases, the I-V characteristics obtained were unique for any given value of I, even when $R \gg d$.

For the first model of Kaplan and Adler (STM), the approximation that $\vec{j} = j_z$ probably uniquely determines the characteristic. Since $T = T_0$ is ambient at the two electrodes, it may be shown that strict application of Maxwell's equations implies uniqueness once a total current I is imposed. Dropping the *curl* condition on the electric field, as they have, probably does not invalidate this point, although we have not yet been able to prove it. However, this is apparently not true for the VEM; it is not clear that a uniqueness proof is possible in this case. As noted above in Sec. V, when the temperature is specified at $r = R$, we expect an I-V characteristic of the type illustrated in Fig. 15 when $R \gg d$ and the problem is solved without the condition $\vec{j} = j_z$. This is in disagreement with their results. In any effect, the condition $\vec{j} = j_z$ acts as a constraint, effectively causing the exclusion of a certain amount of current from the hot interior region of the device. In this way the constraint causes more Joule heating at large values of r where the material is cooled more effectively, so that it appears that at a given imposed field, a greater total current is required through the device to maintain it at the given operating point. We note finally, that this effect does not occur in model B, because, since T is independent of z, the problem caused by lower temperatures near the electrodes does not occur, and a radial flow of current in the device interior is not required to offset this effect.

Another possible contributing factor in the disagreement is the severe restriction on mesh size required in a numerical solution of a two-dimensional problem of this type. If an insufficient number of grid points is utilized, the width of the central hot region will be smeared out, and the resulting current evaluated for a given potential overestimated. It is difficult to determine to what extent either of these points may be contributing factors.

B. Comment on experiment

A fairly detailed picture of the principal features of the MET theory has emerged as a result of the present analysis. Several aspects of the theory not previously understood have been clarified, and it now appears that the predictions of the MET theory agree rather well with experiment. Theory and experiment are worth comparing on several points:

a. Holding voltage and filamentary conduction. For a typical switching device in the conducting state it has been found that the current can be increased or decreased without significantly affecting the voltage drop, normally called the holding voltage, across the device. In this state the dynamic resistance of the device is near zero and conduction appears to be filamentary in character. Furthermore, temperatures in the conducting filament appear to be very high. Gunthersdorfer, for example, has observed a molten area in a 1-μ film of a Te-As-Ge-Si glass by means of a scanning electron microscope and calculated that the temperature had risen by about 500 °K.[75] Armitage *et al.*,[76] Weirauch,[77] and Pearson and Miller[78] have also observed evidence of high filamentary temperatures.

We have seen that the existence of a vertical holding branch to the characteristic on which conduction is filamentary in character is predicted by MET theory. Also, the predicted temperatures in the high-temperature domain are reasonable and appear to agree well with experiment. The positive differential resistance frequently observed in the post switching state is, we believe, due to package resistance. In this state the voltage drop in the electrodes and leads may very well not be negligible as we assumed during the analysis.

b. Holding current. A switching device may be maintained in the conducting state only if a certain current, I_h, called the holding current is maintained. As the current is reduced below this value, the device switches back along the load line to the original highly resistive state. In general it appears that the holding current may or may not be greater than the switching current. This is in essential agreement with our results. In Sec. VI we saw that the vertical holding branch of the characteristic was unstable below a certain current. At lower currents, the high-temperature filament can no longer sustain itself, and the device switches back to the high-resistance state in which the temperature distribution is uniform. The precise location of the point of instability depends upon the load resistance and the particular device configuration.

c. Thickness and temperature dependence of turnaround. Experimental results concerning the thickness and temperature dependence of the switching voltage are in qualitative agreement with the results presented in Sec. IV. Data on the threshold field of a Te-As-Ge-Si glass as a function of thickness from 0.3-1000 μ has been obtained by Kolomiets *et al.*[79]

For films thinner than 5 μ, the threshold field was found to be independent of thickness and to decrease linearly with increasing temperature. Films thicker than 50 μ exhibited a threshold field that varied strongly with temperature and decreased with increasing thickness. Stocker *et al.*[10] also found a thickness-independent region, but only up to about 0.5 μ. For the material and geometries considered here, a typical value of thickness at which the changeover occurs would be 10–20 μ.

Also, in very thin devices, it has been observed that the switching transition disappears, and that the I-V characteristic rises vertically beyond a certain voltage, in agreement with the results of Sec. IV that indicate as $d \to 0$, $V_1 \to V_2$ and the break-back portion of the characteristic becomes vertical. In our case, this would occur typically at $d \lesssim 0.1$ μ.

The experimentally observed loss of switching at high temperatures is in agreement with the results of Sec. IV.

d. Transient "on"-characteristic. We comment here on an experiment reported by Henisch and coworkers.[80,81] In this experiment, a fast rise-time negative-amplitude pulse was applied to a device operating in the on state. In this way it was possible, by varying the height of the pulse, to trace out a transient "on" characteristic. This was done both for devices made with (a) two pyrolytic graphite electrodes, and (b) one pyrolytic and one vitreous graphite electrode. The characteristics obtained in the experiment are represented in Figs. 19(a) and 19(b). At first the characteristic presented in Fig. 19(a) appears puzzling, since it would be expected that the characteristic would go continuously through zero as the pulse is applied. But, in Sec. IV we noted that in the on state predicted by the MET theory, essentially all the field drop occurs at the electrodes, provided they are good heat sinks. Pyrolytic graphite has an extremely high thermal conductivity so that we would expect, in this case, that virtually all the field drop occurs at the electrodes. Since the pulses are of very short duration, the temperature distribution in the device interior doesn't change, and we would expect the characteristic to be given by

$$I \propto V e^{V/d' E_0},$$

where d' is an effective thickness over which the field drop occurs. If we take $d' = 10\%$ of the device thickness (1 μ), we obtain the result presented in Fig. 19(c) for the I-V characteristic when

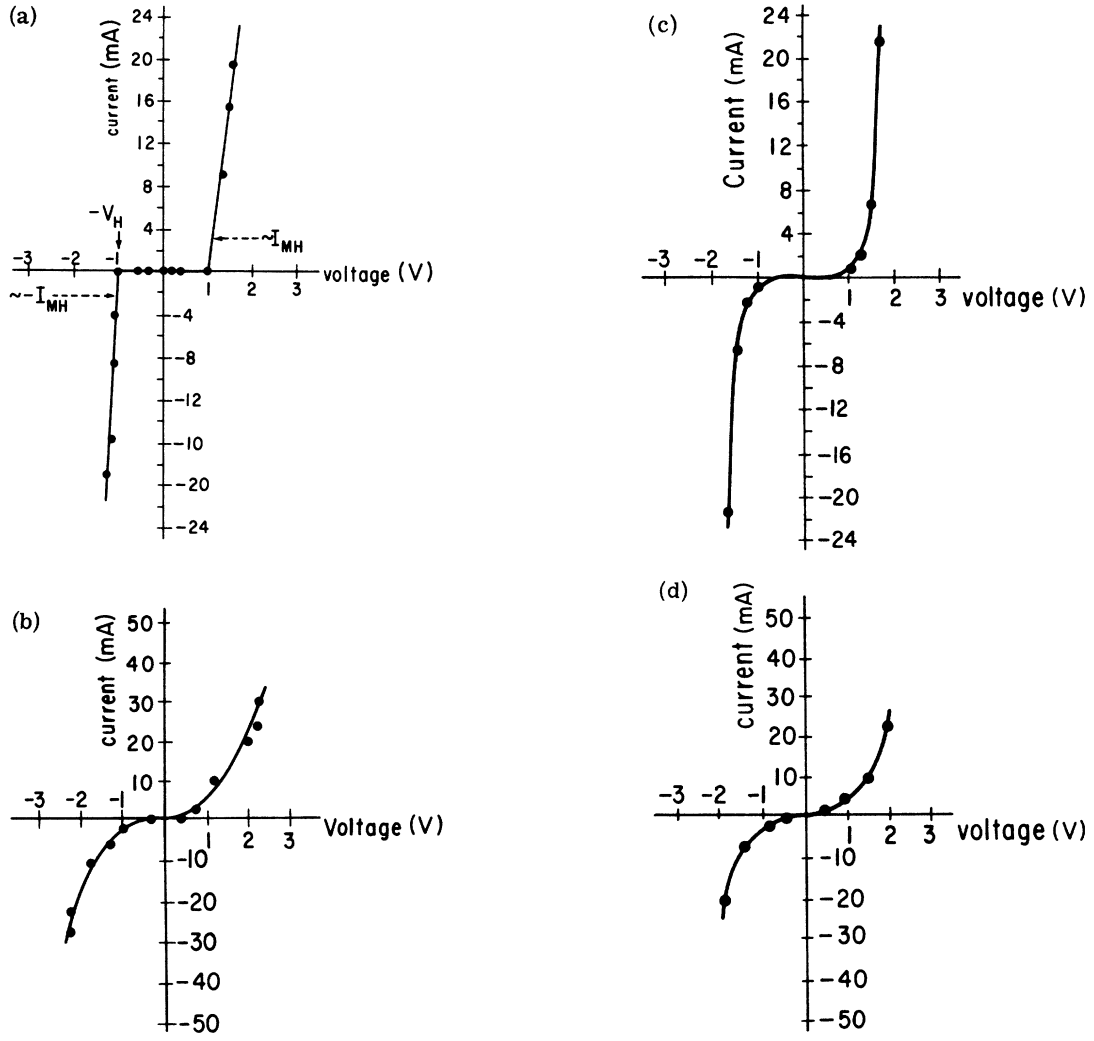

FIG. 19. Transient on characteristics of thin film threshold switches for devices with (a) two pyrolytic graphite electrodes, and (b) one pyrolytic and one vitreous graphite electrode [R. W. Pryor and H. K. Henisch (Ref. 80)]. Characteristic obtaining using $I \propto V\, e^{V/d' E_0}$ for (c) $d' = 0.1d$ and (d) $d' = 0.25d$, $E = 2.2 \times 10^4$ V/cm.

$E_0 = 2.2 \times 10^4$ V/cm. This is seen to agree well with Fig. 19(a).

Turning to the case presented in Fig. 19(b), the thermal conductivity of vitreous graphite is relatively low so that we would expect the effective thickness d' to increase. Results obtained using $d' = 25\%$ of the device thickness are presented in Fig. 19(d). Again the agreement is good, so that it appears reasonable that the result is explainable in terms of the field enhancement at the electrodes due to the high internal temperatures in the conducting channel.

e. Long interrupt on-state (Refs. 81–83). Another result which appears to be at least qualitatively explained by the MET theory is presented in Fig. 20. When two successive pulses are applied to a switch, the threshold voltage of the second pulse is reduced as the interval between pulses is shortened. When the device is switched off for times less than t_s, the hot channel has not had time to diffuse away, and so no switching is experienced upon reapplying the voltage. In the regions B and C of the curve, the gradual increase in the threshold voltage is determined by the extent of diffusion of the hot core. Region A is reached after the hot central region has effectively diffused away. The time constant of 1 μsec for the plateau to be reached is about correct, since this is approximately the thermal relaxation time predicted for these devices. It also appears that the slight increase of V_{th} with time observed in region A may be explained in terms of the slow residual cooling of the

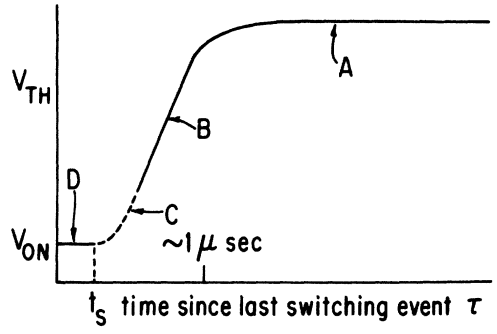

FIG. 20. Long interruption of on state; V_{TH}-vs-t_s relationship. Region A: on state reestablished after switching at the original threshold voltage; Region B: on state reestablished after switching at a reduced threshold voltage; Region C: switch process not well defined; Region D: on state reestablished without switching [Pryor and Henisch (Ref. 80)].

whole device.[83]

It is found experimentally that this V_{th}-vs-τ relation is independent (for $\tau \gtrsim 0.5$ μsec) of ambient temperatures between 200 and 300 °K and of the on current of the first pulse. It is not immediately clear to what extent the MET theory is consistent with these specific results. But since most of the device heat loss is in the axial direction, to the electrodes, and the temperature inside the current channel is independent of the total current through the device (channel diameter), it appears that to a very good approximation the rate at which the hot channel is dissipated should be relatively insensitive to the current level of the initial pulse. Also, the instability and nucleation rate (see below) which determines the threshold voltage or switching delay time depends really upon the temperature difference from ambient, so that qualitatively we would expect the transition between regions A and B to be insensitive to ambient over the range in which $\sigma(T)$ is of the same analytic form. Detailed calculations are required to confirm these ideas, and this explanation must only be taken as tentative at this time.

In addition to this agreement between experiment and theory, there are, however, several recent experimental results which appear not to have a straightforward explanation in terms of the MET theory presented here. These results are very interesting and should prove useful in determining to what extent nonequilibrium or contact effects are important, particularly at temperatures below 300 °K. We briefly outline some of their most important features.

f. Relaxation processes and polarization effects (Refs. 82–84). At low temperatures (down to −78 °C), and to a much lesser extent at room temperature, polarity effects become observable. If, as described above, a device is addressed with a sequence of two pulses, both of sufficient amplitude to cause switching, the threshold voltage of the second pulse is greater if both pulses are of the same polarity than if they are of opposite polarity.[85] Consistent with this result, it has been found that if a device is addressed with periodic switching pulses of constant duration and low frequency (~10–60 Hz) the switching delay time increases with pulse frequency. The reason for the low-frequency requirement here is that higher frequencies would cause device heating, effectively increasing the ambient temperature so that the polarity effects disappear. Furthermore, if at these low temperatures the first pulse is of insufficient height to cause switching, it is found that the threshold voltage of the second pulse is lowered if the pulses are of the same polarity and increased if they are of opposite polarity. This is exactly the opposite effect observed if the first pulse achieves switching. A detailed discussion of these effects is presented in two papers by Henisch and Pryor[82,84] and Burgess and Henisch.[86]

While it may be possible to explain, at least partially, in terms of the present theory the results observed when the first pulse is of insufficient amplitude to cause switching,[87] the results presented when the first pulse does cause switching are exactly the opposite of what we would expect. Certain modifications of the present theory, at least to the extent of including the effects of charge traps, appear necessary if these results are to be explained.

g. Asymmetric electrode effects (Refs. 81 and 88–90). It is well known that for most electrode materials the I-V charactertistic of chalcogenide glass threshold switches is completely symmetric. But recently it has been pointed out that if one or both of the electrodes are made out of a doped crystalline semiconductor (Ge in the present experiments) this is no longer true. In this case, asymmetric switching characteristics are observed; the threshold voltages in the first and third quadrants are different and the on-state characteristics in each of these quadrants is no longer the same. A full discussion of this problem is beyond the scope of the present paper, but it does appear that the effect may be due to more than just rectifying contacts. Detailed calculations of this point need to be performed, though, since the prethreshold characteristic agrees rather well with a simple rectifying contact model. Proper treatment of the postswitching state requires channeled current flow and subsequent extensive heating of the semiconductor contacts so that it is not clear what the on-state characteristic should look like. A satisfactory explanation of both the

static and transient characteristics of these devices with asymmetric contacts does not exist.

Therefore, although the present theory accounts rather well for all the "primary" switching characteristics observed, it appears that contact, injection, and trapping effects must play some role in explaining certain of the asymmetric electrode effects and polarization and relaxation processes outline above. Further improvements of the present theory are required in these cases.

Finally, we consider a possible interpretation of the actual switching event.

C. Nucleation theory of switching

It is well known that the character of the switching event in chalcogenide glass threshold switches is different for small and large overvoltages. For voltages close to threshold the switching delay time is subject to substantial fluctuations. This is not the case when large overvoltages are applied. For large overvoltages the switching event loses its statistical character and it has already been shown in this case that the observed dependence of delay time on overvoltage is in good agreement with the predictions of electrothermal theories.[13] Figure 21 clearly illustrates these two regions.[91,92]

For small overvoltages it may be shown that the observed statistical distribution in switching voltages in these devices is consistent with nucleation with a time-independent, but voltage-dependent probability.[93] Because of this we are led to the following interpretation of the switching event. We have seen previously that for voltages not too far below turnaround, an unstable branch of the I-V characteristic determined by radially dependent temperature and current distributions (branch c in Fig. 17), lies very close to the "off" state (branch a in Fig. 17). This branch forms a "separatrix" between the off and on states. Temperature and current fluctuations of sufficient size to carry the system along the load line across this branch will cause switching to occur. As the turnaround voltage is approached, the required size of the fluctuations decreases (see Fig. 14). We are led in this way to the concept of nucleation and growth of a hot spot in the device interior as the cause of switching.

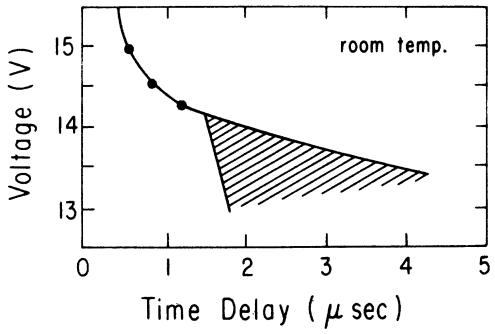

FIG. 21. Relationship between applied voltage and switching delay time t_D for threshold switch. (S. H. Lee, H. K. Henisch, and W. D. Burgess.[91])

For $V < V_1$, where V_1 is the turnaround voltage, the switching would be statistical in character, the portion of the characteristic below turnaround being metastable. For $V > V_1$, the current and temperature distribution in the device is unstable with respect to infinitesimal perturbations and the switching event is no longer statistical in character. Thus a determination of the voltage at which fluctuations in delay time ceased could give a good value for the turnaround voltage. For geometries in which the separation between branches a and c of the characteristic are greater, we would expect the delay time for $V < V_1$ to increase considerably. When this separation becomes great enough, we would finally expect no switching to be observed for $V < V_1$.

Finally, we note that in this model, the switching delay time is explained in terms of the time it takes a fluctuation to reach critical size, i.e., attain a size on the order of the device thickness. This should be somewhat greater than the thermal relaxation time for these devices, about 1 μsec. Once a critical fluctuation is achieved, the energy stored in the circuit discharges through the embryonic channel, heating the material and switching the device. This last event can take place very rapidly, on the order of 10^{-10} sec.[13,46]

We are presently studying the dynamical behavior of critical fluctuations in nonequilibrium macroscopic systems in an attempt to determine if the above hypothesis is indeed correct.

We close with a brief review of a full switching cycle predicted by a synthesis of the above results (Fig. 17). As the applied voltage is increased in the off state we trace out portion a of the characteristic. Switching is initiated at some point not too far below turnaround as the result of a macroscopic critical fluctuation.

Once switching is initiated, the device discharges through the embryonic channel and switches along the load line to the stable vertical portion of branch d. Here virtually all the current flow is carried in a hot channel. As the current through the device is decreased branch d is traced out until shortly before point 5 is reached. Below this point branch d is unstable and we switch back along the load line to branch a by a similar process of nucleation and growth, but now of a cold region.

ACKNOWLEDGMENTS

I am deeply indebted to Professor Morrel H. Cohen for his continued assistance and guidance.

I also wish to thank everyone in the solid-state-theory group at The University of Chicago for continued assistance, and J. Evans, R. Landauer, and F. Stern for reasons already mentioned in the text.

APPENDIX A

For radially uniform solutions the steady-state form of Eqs. (1)–(3) reduces to

$$\frac{d}{dz}\left[K\left(T, \frac{d\phi}{dz}\right)\frac{dT}{dz}\right] + j\frac{d\phi}{dz} = 0, \tag{A1}$$

$$\sigma = \sigma(T)\, e^{|\frac{d\phi}{dz}|/E_0}, \tag{A2}$$

$$j = \sigma\left(T, \frac{d\phi}{dz}\right)\frac{d\phi}{dz}, \tag{A3}$$

in domain $D = (-\frac{1}{2}d, \frac{1}{2}d)$, and

$$K\frac{dT}{dz} + \alpha T = \alpha T_0, \quad z = \pm\tfrac{1}{2}d. \tag{A4}$$

The divergence condition on the current becomes $dj/dz = 0$, so that the current density is constant in D. Also, to simplify notation we write $E = d\phi/dz$.

We shall show that the system (A1)–(A4) possesses a unique solution for any imposed positive current density. Equivalently, the I-V characteristic obtained by solution of Eqs. (A1)–(A4) is unique.

Since j is a constant and both the partial derivatives of $\sigma(T, E)E$ with respect to T and E are positive definite for all T and E greater than zero, the implicit function theorem permits us to solve Eqs. (A2) and (A3) uniquely for E in terms of T for any given j. If we write $E = E(T)$, therefore, the system (A1)–(A4) reduces to

$$\frac{d}{dz}\left[K(T)\frac{dT}{dz}\right] + jE = 0, \quad z \in D \tag{A5}$$

$$K(T)\frac{dT}{dz} + \alpha T = \alpha T_0, \qquad z = \pm\tfrac{1}{2}d \tag{A6}$$

$$j = \text{const}. \tag{A7}$$

Also, $K(T)$ is a monotonically increasing function of T for any given j:

$$\frac{dK}{dT} = \frac{d}{dT}[K_1 + K'\sigma(T, E)T] = K'\left(\frac{d\sigma}{dT}T + \sigma\right) > 0,$$

since by Eq. (A2)

$$\frac{d\sigma}{dT}(T, E) = \frac{\sigma(T, E)}{E_0}\frac{\partial E}{\partial T} + \frac{\partial\sigma(T, E)}{\partial T}$$

and by Eqs. (A3) and (A7)

$$\left(1 + \frac{E}{E_0}\right)\sigma(T, E)\frac{\partial E}{\partial T} + E\frac{\partial\sigma(T, E)}{\partial T} = 0,$$

so that we have

$$\frac{d\sigma(T, E)}{dT} = \frac{\partial\sigma(T, E)}{\partial T} - \frac{E}{E_0}\frac{1}{(1 + E/E_0)}\frac{\partial\sigma(T, E)}{\partial T}$$

$$= \frac{1}{(1 + E/E_0)}\frac{\partial\sigma(T, E)}{\partial T} > 0$$

since $\partial\sigma/\partial T > 0$. Because $K(T)$ is a monotonic function of T, it is useful to make the change of variable

$$u = \int_0^T K(\tau)\, d\tau\,.$$

u is a uniquely defined function of T, and a unique inverse exists. In terms of u, Eqs. (A5) and (A6) may be rewritten

$$\frac{d^2u}{dz^2} + jE[T(u)] = 0, \quad z \in D \tag{A8}$$

$$\frac{du}{dz} + \alpha T[u] = \alpha T_0, \quad z = \pm\tfrac{1}{2}d. \tag{A9}$$

We now consider the equivalent problem of extremizing the functional

$$I = \int_{-d/2}^{d/2} dz \left\{\frac{1}{2}\left(\frac{d\Phi}{dz}\right)^2 + \alpha T[\Phi]\frac{d\Phi}{dz} - \alpha T_0\frac{d\Phi}{dz} - j\int^{\Phi} E(\Psi)\, d\Psi\right\} = \int dz F\left[z, \Phi, \frac{d\Phi}{dz}\right]. \tag{A10}$$

We seek to minimize (A10) over the set of all functions which are positive and possess continuous second derivatives in domain D. This requires that the first variation of I with respect to Φ be zero. Setting $\Phi(z) = u(z) + \epsilon\eta(z)$, we differentiate (A10) with respect to ϵ once and set the limit, as $\epsilon \to 0$, of this expression equal to zero. Thus,

$$\delta I(\epsilon = 0) = \int_{-d/2}^{d/2} dz \left(\frac{du}{dz}\eta_z + \alpha\frac{dT}{du}\frac{du}{dz}\eta + \alpha T\eta_z - \alpha T_0\eta_z - jE[u]\eta\right) = 0$$

or

$$\left(\frac{du}{dz} + \alpha T[u] - \alpha T_0\right)\eta\Big|_{-d/2}^{d/2} + \int_{-d/2}^{d/2} dz \left(-\frac{d^2u}{dz^2} - jE[u]\right)\eta = 0 \tag{A11}$$

after integration by parts.

The first expression on the left-hand side gives the transversality conditions corresponding to the boundary conditions (A9), while the integrand of the second term is just equation (A8), the Euler's equation for (A10), so that by standard arguments, u is a solution of the system (A8) and (A9) if and only if it extremizes (A10).

Differentiating (A10) twice with respect to ϵ and taking the limit,

$$\delta^2 I(\epsilon=0)=\int_{-d/2}^{d/2} dz\left[(\eta_z)^2+\alpha\left(\frac{d^2T}{du^2}\right)\frac{du}{dz}\eta^2+2\alpha\frac{dT}{du}\eta\eta_z+\alpha T[u]\eta_z^2-j\frac{dE}{du}\eta^2\right]$$

$$=\int_{-d/2}^{d/2} dz\left[\eta_z^2+\frac{d}{dz}\left(\alpha\frac{dT}{du}\eta^2\right)+\alpha T[u]\eta_z^2-j\frac{dE}{du}\eta^2\right]$$

$$=\alpha\frac{dT}{du}\eta^2\Big|_{-d/2}^{d/2}+\int_{-d/2}^{d/2} dz\left[(1+\alpha T[u])\eta_z^2-j\frac{dE}{du}\eta^2\right]. \tag{A12}$$

The first term in (A12) is zero because of the symmetry of the boundary conditions. Also,

$$\frac{dE}{du}=\frac{dE}{dT}\frac{dT}{du}$$

$$=-E\frac{\partial\sigma(T,E)}{\partial T}\left[K(T,E)\sigma(T,E)\left(1+\frac{E}{E_0}\right)\right]^{-1}<0,$$

so that

$$\delta^2 I(\epsilon=0)=\int_{-d/2}^{d/2} dz\left((1+\alpha T[u])\eta_z^2-j\frac{dE}{du}\eta^2\right)>0$$

for *all* functions u which are greater than zero and twice continuously differentiable in D. Therefore, I is concave upwards over the set of all admissible functions.

Thus we have only one solution for any given j, since a functional which is everywhere concave upwards can have at most one stationary point, a minimum.

APPENDIX B

We consider here the question of existence of entire solutions of the equation

$$\frac{1}{r}\frac{d}{dr}\left(r\frac{du}{dr}\right)-a(u-u_0)+bf(u)=0 \tag{B1}$$

in which a, u_0, and b are constants. $f(u)$ is assumed to possess property A:

$$\frac{df}{du}\geq 0,\quad u\in(0,\infty)$$

$$\frac{d^2f}{du^2}>0,\quad u\in(0,\bar{u}),\quad \bar{u}>u_0$$

$$\frac{d^2f}{du^2}<0,\quad u\in(\bar{u},\infty).$$

The analogy of this problem with the model system B considered in the text is obvious.

Because of property A, the relation

$$-a(u-u_0)+bf(u)=0 \tag{B2}$$

possesses three solutions for $b\in(b_1, b_2)$, where b_1 and b_2 are the simultaneous solutions of the system (B2) and

$$b\frac{df}{du}-a=0. \tag{B3}$$

This behavior is demonstrated in Fig. 22(a).

Therefore, for $b^*\in(b_1, b_2)$ the function

$$g(U)=\int_0^U[-a(u-u_0)+b^*f(u)]\,du$$

possesses three extrema at u_1, u_2, and u_3, given by the solutions of (B2) with $b=b^*$ [see Fig. 22(b)], and there clearly exist $u'\in(u_1, u_2)$, $u''\in(u_2, u_3)$ such that

$$g(u')-g(u'')=0. \tag{B4}$$

Consider now the equation

$$\frac{d^2u}{dr^2}-a(u-u_0)+b^*f(u)=0 \tag{B5}$$

in the domain $(0,\infty)$. Multiplying (B5) by du/dr,

$$\frac{du}{dr}\frac{d^2u}{dr^2}+[-a(u-u_0)+b^*f(u)]\frac{du}{dr}=0$$

or

$$\frac{d}{dr}\left\{\frac{1}{2}\left(\frac{du}{dr}\right)^2+\int^u[-a(u'-u_0)+b^*f(u')]\,du'\right\}=0.$$

Integrating from 0 to r, we get

$$\frac{1}{2}\left(\frac{du}{dr}\right)^2+g[u(r)]-g[u(0)]=0$$

if we require that $(du/dr)|_0=0$, so that

$$\frac{du}{dr}=\pm\sqrt{2}\{g[u(0)]-g[u(r)]\}^{1/2}. \tag{B6}$$

If we take $u(0)=u''$, Eq. (B6) clearly possesses an entire oscillating solution, the sign of the right-hand side of (B6) changing every time $u(r)$ goes through u' or u''.

Returning to (B1), we multiply it by du/dr and integrate from 0 to r, getting

$$\frac{1}{2}\left(\frac{du}{dr}\right)^2+\int_0^r\left(\frac{du}{dr'}\right)^2\frac{dr'}{r'}+g[u(r)]-g[u(0)]=0, \tag{B7}$$

since $(du/dr)|_0=0$. Because $\int_0^r(du/dr')^2dr'/r'\geq 0$, Eq. (B7) yields

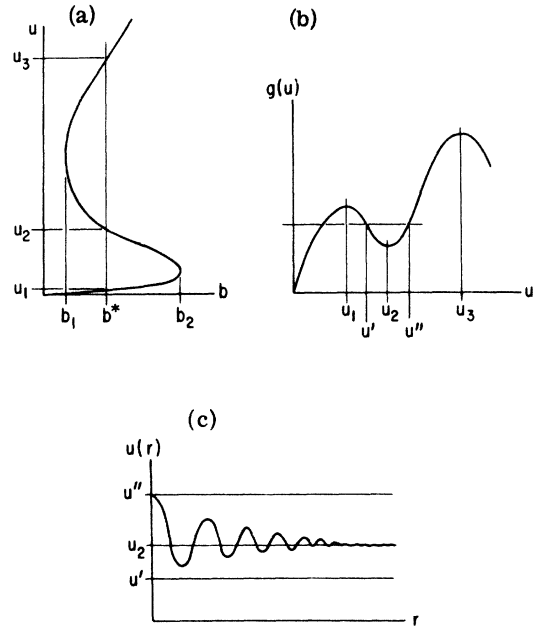

FIG. 22. (a) u–b plot of solutions to Eq. (B2); (b) $g(u)$ vs u for $b = b^*$; (c) entire damped oscillatory solution to Eq. (B1) for $u(0) = u''$.

$$\frac{1}{2}\left(\frac{du}{dr}\right)^2 + g\,[u(r)] - g\,[u(0)] \leq 0$$

or

$$\left|\frac{du}{dr}\right| \leq \sqrt{2}\,\{g[u(0)] - g[u(r)]\}^{1/2}\,, \tag{B8}$$

which possesses a damped oscillatory solution if $u(0) = u''$ where u'' is such that a $u' \in (u_1, u_2)$ exists which satisfies (B4). Note that $u(r) \to u_2$ as $r \to \infty$, and that

$$u_3 > u(r) > u_1 > u_0$$

for all $r \geq 0$. This solution is illustrated in Fig. 22(c) for $u'' > u'$.

APPENDIX C

The system

$$\frac{K}{r}\frac{d}{dr}\left(r\frac{dT}{dr}\right) - \alpha(T - T_0) + \sigma(T, E)E^2 = 0\,, \tag{C1}$$

$$T(0)\ \text{(finite)},\quad \left.\frac{dT}{dr}\right|_R = 0\,, \tag{C2}$$

where $\alpha = 8K/d^2$ has at least one solution corresponding to a uniform temperature distribution $T(E)$ for any $E > 0$. We now seek solutions of Eqs. (C1) and (C2) other than $T(E)$ using a perturbation technique described in a series of papers by Keller, Millman, and Ting.[64–66]

We seek a one-parameter family of solutions $E(\epsilon)$ and $T(r, \epsilon)$ which depend differentially on an amplitude parameter ϵ and reduce to the uniform solution E, $T(E)$ for $\epsilon = 0$. Both T and E will be assumed to be sufficiently differentiable with respect to ϵ at $\epsilon = 0$ that they may be expanded in a Taylor series about this point:

$$T(r, \epsilon) = T + \epsilon T' + \tfrac{1}{2}\epsilon^2 T'' + \cdots\,, \tag{C3}$$

$$E(\epsilon) = E + \epsilon E' + \tfrac{1}{2}\epsilon^2 E'' + \cdots\,. \tag{C4}$$

In more general terms, what we are interested in is the process of bifurcation whereby a given solution of Eqs. (C1) and (C2) splits up into two or more solutions as E passes through a critical value E^*, called a bifurcation point. The main problem is to determine the properties of these solutions and how they depend upon E.

We denote the uniform solution by T and E, and, as in (C3) and (C4), denote by $T'(r)$, E', $T''(r)$, E'', etc., the derivatives of $T(r, \epsilon)$ and $E(\epsilon)$ with respect to ϵ at $\epsilon = 0$. In general, the equations governing the coefficients in the expansion are obtained by differentiating (C1) and (C2) with respect to ϵ and setting $\epsilon = 0$.

Differentiating once, we obtain

$$\frac{d}{dr}\left(r\frac{dT'}{dr}\right) + r\left(\frac{\partial\sigma}{\partial T}E^2 - \alpha\right)K^{-1}T' = -\frac{r}{K}\left(2 + \frac{E}{E_0}\right)\sigma E E''\,, \tag{C5}$$

$$T'(0)\ \text{(finite)},\quad \text{and}\quad \left.\frac{dT'}{dr}\right|_R = 0\,. \tag{C6}$$

If we assume that $(\partial\sigma/\partial T)E^2 - \alpha \neq 0$, then (C5) and (C6) constitute a linear inhomogeneous eigenvalue problem for $k^2 = [(\partial\sigma/\partial T)E^2 - \alpha]/K$ and $T'(r)$. The homogeneous system, corresponding to (C5) and (C6), constitutes a Sturm-Liouville problem and therefore possesses a complete set of eigenvalues k_n^2 and orthonormal eigenfunctions $\phi_0(k_n r)$ (the zero-order Bessel functions). The homogeneous system possesses a solution whenever

$$k_n^2 = \left(\frac{\partial\sigma}{\partial T}E^2 - \alpha\right)K^{-1}\,,$$

k_n such that $J_1(k_n R) = 0$, so that solutions only exist for $(\partial\sigma/\partial T)E^2 - \alpha > 0$, i.e., on the negative differential conductivity portion of the I-V characteristic. Clearly, bifurcation can only occur at solutions of the linearized problem.

The inhomogeneous form of (C5) has a solution only if the right-hand side is orthogonal to $\phi_0(k_n r)$, when $k_n^2 = [(\partial\sigma/\partial T)E^2 - \alpha]/K$. To see this, multiply

$$\frac{d}{dr}\left(r\frac{dT'}{dr}\right) + r k_n^2 T' = -f(r)r$$

by $\phi_0(k_n r)$ and integrate from 0 to R:

$$-\int_0^R r\,dr f(r)\phi_0(k_n r)$$

$$= \int_0^R \phi_0(k_n r)\left[\frac{d}{dr}\left(r\frac{dT'}{dr}\right) + r k_n^2 T'\right]$$

$$= \int_0^R \left[\frac{d}{dr}\left(r\frac{d\phi_0}{dr}\right) + r k_n^2 \phi_0\right] T' \, dr = 0 .$$

This condition is trivially satisfied in the case of (C5) and (C6) since the right-hand side is a constant, and

$$\int_0^R r\,dr\, J_0(k_n r) = (R/k_n) J_1(k_n R) = 0 .$$

The complete solution of (C5) and (C6) is therefore

$$T_n'(r) = A\phi_0(k_n r) - \frac{(2 + E/E_0)\sigma E}{k_n^2 K} E_n' , \qquad \text{(C7)}$$

where

$$k_n^2 = \left(\frac{\partial\sigma}{\partial T}E^2 - \alpha\right)\Big/ K . \qquad \text{(C8)}$$

The amplitude factor A is not yet uniquely defined since we may add to (C7) any solution of the homogeneous problem. But by defining ϵ appropriately we may arrange that $A = 1$. Millman and Keller[65] have shown that a suitable definition of ϵ for this purpose is

$$\epsilon = \int_0^R r\,dr\,[T'(r) + \gamma E'] \times [T(r, \epsilon) + \epsilon\gamma E' - T], \qquad \text{(C9)}$$

where $\gamma = (2 + E/E_0)\sigma E/Kk^2$. Differentiating (C9) with respect to ϵ and then setting $\epsilon = 0$, we have

$$1 = \int_0^R r\,dr\,[T'(r) + \gamma E']^2 . \qquad \text{(C10)}$$

From this it follows that $A^2 = 1$, so that $A = \pm 1$. Only the product ϵA appears in the expansion of T, so that we may choose $A = 1$. Therefore $T_n'(r)$ is uniquely defined as

$$T_n'(r) = \phi_0(k_n r) - \gamma E_n' . \qquad \text{(C7a)}$$

Differentiating (C1) and (C2) j times with respect to ϵ and taking the limit $\epsilon \to 0$ gives an inhomogeneous eigenvalue problem for $T^{(j)}(r)$. Doing the same to (C9) gives us

$$\int_0^R r\,dr(T' + \gamma E')\,T^{(j)}(r) = 0 . \qquad \text{(C11)}$$

These three equations suffice to define $T^{(j)}$ and $E^{(j)}$ uniquely.

A sequence of solutions $T'(r)$ are defined in the above manner, and since the uniform solutions satisfy

$$-\alpha(T - T_0) + \sigma(T, E)E^2 = 0 , \qquad \text{(C12)}$$

(C8) suffices to determine the critical values of E and T about which solutions (C7) exist.

The solution $T'(r)$ we shall be primarily concerned with is the one corresponding to k_1, i.e., the lowest mode. This solution has no nodes, so that T' decreases monotonically for $r \in (0, R)$. This solution lies "lowest" on the I-V characteristic, closest to the point of voltage turnaround. The higher modes contain an increasing number of nodes and lie at progressively higher currents. The number of critical values [Eqs. (C1) and (C2)] determined depends in detail on K, σ, α, the device radius, and thickness (Fig. 23).

Differentiating (C1) twice with respect to ϵ and setting $\epsilon = 0$ we get

$$\frac{d}{dr}\left(r\frac{dT''}{dr}\right) + \frac{r}{K}\left(\frac{\partial\sigma}{\partial T}E^2 - \alpha\right)T''$$

$$= -\frac{r}{K}\left[\sigma E\left(2 + \frac{E}{E_0}\right)E'' + \left(2 + 4\frac{E}{E_0} + \frac{E^2}{E_0^2}\right)\sigma E'^2 + 2E\left(2 + \frac{E}{E_0}\right)\frac{\partial\sigma}{\partial T}E'T' + E^2\frac{\partial^2\sigma}{\partial T^2}T'^2\right], \qquad \text{(C13)}$$

$$T''(0)\,\text{(finite)}, \quad \text{and} \quad \left.\frac{dT''}{dr}\right|_R = 0 . \qquad \text{(C14)}$$

This again is an inhomogeneous, linear eigenvalue problem for $T''(r)$. If it is to have a solution for a given value k^2 of $(\partial\sigma/\partial T)E^2 - \alpha$, the right-hand side of (C13) must be orthogonal to $\phi_0(kr)$. This solvability criterion implies that, if (C7a) is used for $T(r)$,

$$2E\left(2 + \frac{E}{E_0}\right)\frac{\partial\sigma}{\partial T}E' + E^2\frac{\partial^2\sigma}{\partial T^2}\int_0^R r\,dr \times \phi_0^3(kr) - 2\gamma E^2\frac{\partial^2\sigma}{\partial T^2}E' = 0$$

or

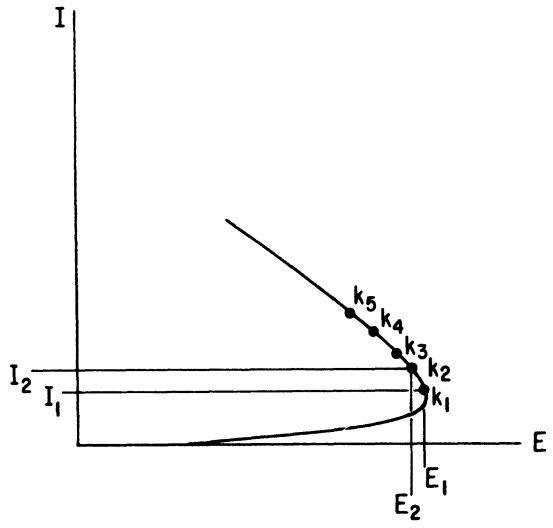

FIG. 23. Schematic I-V plot showing relative location of successive hifurcation points for $R \gg d$.

$$E' = -E\frac{\partial^2\sigma}{\partial T^2}\int_0^R r\,dr\,\phi_0^3(kr) \times\left(2\frac{\partial\sigma}{\partial T}\left(2+\frac{E}{E_0}\right)\left\{1-\left[\frac{\partial^2\sigma}{\partial T^2}\Big/\left(\frac{\partial\sigma}{\partial T}\right)^2\right]\right. \times\left.\left(\sigma\frac{\partial\sigma}{\partial T}E^2\Big/Kk^2\right)\right)^{-1} \tag{C15}$$

In this way E' is uniquely determined by our choice of normalization for $T(r)$. When E' is given by (C15), the system (C13) and (C14) has a solution $T''(r)$, which is unique because of (C11). $T''(r)$ may be expressed in terms of the modified Green's function defined by

$$\frac{d}{dr'}\left(r'\frac{d}{dr'}G(r,r')\right)+k^2r'G(r,r') = -\delta(r-r')+r'\phi_0(kr)\phi_0(kr'), \tag{C16}$$

$$\left.\frac{dG(r,r')}{dr}\right|_R = 0, \tag{C17}$$

$$\int_0^R G(r,r')\phi_0(kr)\,r\,dr = 0, \tag{C18}$$

where (C18) guarantees that T'' will satisfy (C11).

This modified Green's function for the present problem is

$$G(r,r') = \frac{\beta^2}{2k}\left(\frac{rJ_1(kr)Y_1(kR)-RY_0(kR)J_0(kr)+RJ_0(kR)Y_0(kr)}{Y_1(kR)}\right)J_0(kr')+\frac{\beta^2}{2k}r'J_0(kr)J_0(kr'), \qquad 0\le r'<r$$

$$G(r,r') = \frac{\beta^2}{2k}\left(rJ_1(kr)-R\frac{Y_0(kR)}{Y_1(kR)}J_0(kr)\right)J_0(kr')+\frac{\beta^2}{2k}R\frac{J_0(kR)}{Y_1(kR)}J_0(kr)Y_0(kr')+\frac{\beta^2}{2k}r'J_0(kr)J_0(kr'), \quad r<r'\le R$$

where $\beta^2 = 2/R^2J_0^2(kR)$ is the normalization factor for $J_0(kr)$. Applying G to the right-hand side of (C13) we get

$$T''(r) = -\sigma E\left(2+\frac{E}{E_0}\right)\Big/k^2K\Big]E'' -\left[\sigma\left(2+4\frac{E}{E_0}+\frac{E^2}{E_0^2}\right)\Big/k^2K\right]E'^2+\left[2E\frac{\partial\sigma}{\partial T}\gamma\left(2+\frac{E}{E_0}\right)\Big/k^2K\right]E'^2 -\left(\frac{\partial^2\sigma}{\partial T^2}\gamma^2E^2\Big/k^2K\right)E'^2+\frac{\partial^2\sigma}{\partial T^2}\frac{E^2}{2k^2K}\frac{\partial^2\sigma}{\partial T^2}B, \tag{C19}$$

where

$$B = \beta^4k\left[\left(rJ_1(kr)-R\frac{Y_0(kR)}{Y_1(kR)}J_0(kr)\right)\int_0^R y\,dy\,J_0^3(ky)+R\frac{J_0(kR)}{Y_1(kR)}\left(Y_0(kr)\int_0^R y\,dy\,J_0^3(ky) +J_0(kr)\int_r^R y\,dy\,Y_0(ky)J_0^2(ky)\right)+J_0(kr)\int_0^R y^2\,dy\,J_1(ky)J_0^2(ky)\right].$$

Differentiating (C1) and (C2) three times with respect to ϵ and setting $\epsilon = 0$ we have

$$\frac{d}{dr}\left(r\frac{dT'''}{dr}\right)+\left[\left(\frac{\partial\sigma}{\partial T}E^2-\alpha\right)\Big/K\right]rT''' = -\frac{r}{K}\left[3\sigma\left(2+4\frac{E}{E_0}+\frac{E^2}{E_0^2}\right)E'E''+\frac{\sigma}{E_0}\left(6+6\frac{E}{E_0}+\frac{E^2}{E_0^2}\right)E'^2 +\sigma\left(2+\frac{E}{E_0}\right)EE'''+3\frac{\partial\sigma}{\partial T}E\left(2+\frac{E}{E_0}\right)E''T'+3\frac{\partial\sigma}{\partial T}\left(2+4\frac{E}{E_0}+\frac{E^2}{E_0^2}\right)E'^2T'+3\frac{\partial^2\sigma}{\partial T^2}\left(2E+\frac{E^2}{E_0}\right)E\,T'^2 +3\frac{\partial\sigma}{\partial T}\left(2E+\frac{E^2}{E_0}\right)E'T''+3E^2\frac{\partial^2\sigma}{\partial T^2}T'T''+\frac{\partial^3\sigma}{\partial T^3}E^2T'^3\right]. \tag{C20}$$

This is again an inhomogeneous form of the system considered above. Using the solvability condition we get a unique expression for E''. Reinserting this value of E'', there is a unique $T'''(r)$ determined by the integral of $G(r,r')$ multiplied by the right-hand side of (C20). In this manner it is possible to determine successive coefficients in the expansion [Eqs. (C3) and (C4)].

Collecting results, we see that for each positive integer n we have obtained a one-parameter family of solutions of Eqs. (C1) and (C2) provided that the linearized equations given by the homogeneous part of (C5) and (C6) possess a solution at some E for a uniform temperature distribution $T(E)$. These solutions are given by the expressions

$$T(r,\epsilon) = T+\epsilon T'(r)+\tfrac{1}{2}\epsilon^2T''(r)+\cdots,$$

$$E(\epsilon) = E+\epsilon E'+\tfrac{1}{2}\epsilon^2E''+\cdots.$$

In a similar manner the current

$$I=2\pi\int_0^R r\,dr\,j(r)=2\pi\int_0^R r\,dr\,\sigma[T(r,\epsilon),E(\epsilon)]E(\epsilon) \tag{C21}$$

may be expanded as a power series in ϵ about the nth bifurcation point. Expanding, using (C3) and (C4), we have

$$I(\epsilon)=I_0+\epsilon I'+\tfrac{1}{2}\epsilon^2 I''+\cdots, \tag{C22}$$

where

$$I_0=\pi R^2\sigma E,$$

$$I'=\pi R^2\sigma\left(1+\frac{E}{E_0}\right)\times\left\{1-\left[\left(2+\frac{E}{E_0}\right)\Big/\left(1+\frac{E}{E_0}\right)\right]\left(\frac{\partial\sigma}{\partial T}E^2\Big/k^2K\right)\right\}E',$$

$$I''=2\pi\int_0^R r\,dr\left[\sigma\left(1+\frac{E}{E_0}\right)E''+2\frac{\partial\sigma}{\partial T}\left(1+\frac{E}{E_0}\right)E'T'(r)+\frac{\partial\sigma}{\partial T}ET''(r)+\frac{\partial^2\sigma}{\partial T^2}ET'^2(r)+\frac{\sigma}{E_0}\left(2+\frac{E}{E_0}\right)E'^2\right].$$

If the solutions to (C5) and (C6) of the form (C7) and (C8) exist, then solutions of (C1) and (C2), corresponding to radially dependent temperature distributions, exist and bifurcate from the critical points E, T determined by (C8). Equations (C3), (C4), and (C22) uniquely characterize these solutions in the neighborhood of the bifurcation points.

APPENDIX D

We have seen that the system

$$\vec{\nabla}\cdot(K\vec{\nabla}T)+\vec{j}\cdot\vec{E}=0, \tag{D1}$$

$$\vec{\nabla}\cdot\vec{j}=0, \tag{D2}$$

$$\vec{\nabla}\times\vec{E}=0, \tag{D3}$$

$$\vec{j}=\sigma(T)\vec{E}\,e^{|E|/E_0} \tag{D4}$$

$$\vec{x}\in D\{(r,\phi,z)\,|\,0\le r<R,\ 0\le\phi<2\pi,\ -\tfrac{1}{2}d<z<\tfrac{1}{2}d\}$$

$$T(r,z)\Big|_{\pm d/2}=T_0,\quad \frac{\partial T}{\partial r}\Big|_R=0 \tag{D5}$$

$$\vec{j}\cdot r\,|_R=0,\quad j_r(r,z)|_{\pm d/2}=0 \tag{D6}$$

possesses a solution corresponding to a radially uniform temperature distribution for all applied currents I, and that this solution is unique if we restrict ourselves to one dimension (no r dependence). The I-V characteristic, corresponding to this set of solutions when the constitutive relation (D4) is used, possesses a break-back region in which $dI/dV<0$. Analogy with the results of Appendix C, and the fact that it does not appear possible to prove a uniqueness theorem of the above type when we remove the one-dimensional restriction if the I-V characteristic for the constrained one-dimensional solutions possesses negative differential conductivity behavior, leads us to believe that other radially-dependent solutions to (D1)–(D6) exist. Our objective is to determine the criterion for the existence of such solutions and their behavior in a neighborhood of the previously determined one-dimensional solutions.

We seek a one-parameter family of solutions $T(r,z,\epsilon)$, $\vec{j}(r,z,\epsilon)$, etc., which depend differentially on an amplitude parameter ϵ and which reduce to the radially uniform solution for $\epsilon=0$. We shall attempt to represent these solutions in a Taylor series in ϵ about $\epsilon=0$. The procedure is the same as that used in Appendix C.

We restrict ourselves to the two-dimensional cylindrically symmetric case so that the current $\vec{j}$ may be represented by

$$\vec{j}=-\operatorname{curl}(\psi/r)\hat{\phi},$$

where $\hat{\phi}$ is the unit polar vector. The thermal conductivity K will be taken as constant (this is a realistic assumption in the temperature ranges we are interested in here, less than 500 °K) and we seek to express T and ψ in the form

$$T(r,z,\epsilon)=T(z)+\epsilon T'(r,z)+\frac{\epsilon^2}{2}T''(r,z)+\cdots, \tag{D7}$$

$$\psi(r,z,\epsilon)=-(\alpha_0+\epsilon\alpha'+\tfrac{1}{2}\epsilon^2\alpha''+\cdots)\tfrac{1}{2}r^2+\epsilon\psi'(r)+\tfrac{1}{2}\epsilon^2\psi''(r)+\cdots. \tag{D8}$$

The α's are constants and constitute the radially uniform contribution to the current density by $\psi(r,z,\epsilon)$. The first terms in the expansion are to be identified with the radially uniform solutions to Eqs. (D1)–(D6).

In general, the equations governing the coefficients in the expansions (D7) and (D8) are obtained by differentiating Eqs. (D1)–(D6) with respect to ϵ and setting $\epsilon=0$. Differentiating once, we obtain

$$K\nabla^2T'-A\frac{\psi'_r}{r}-BT'=-A\alpha', \tag{D9}$$

$$\frac{\partial}{\partial r}\left(C\frac{\psi'_r}{r}+DT'\right)+\frac{\partial}{\partial z}\left(\frac{\psi'_z}{r\sigma}\right)=\frac{\partial}{\partial r}(\alpha'C), \tag{D10}$$

where

$$A=E(2+E/E_0)/(1+E/E_0), \tag{D11}$$

$$B=\frac{\partial\sigma}{\partial T}\frac{E^2}{(1+E/E_0)}, \tag{D12}$$

$$C=\frac{1}{\sigma(1+E/E_0)}, \tag{D13}$$

$$D=\frac{1}{\sigma}\frac{\partial\sigma}{\partial T}\frac{E}{1+E/E_0}, \tag{D14}$$

and $\sigma=\sigma(T,E)$, $E=d\phi/dz$.

Bifurcation is possible only if the system (D9)

and (D10) possesses a solution. In general, the problem of obtaining the solution of (D9) and (D10) is quite difficult because of the z dependence of the coefficients. But, because of the strong field dependence of the conductivity, and the fact that peak central temperatures near the voltage turnaround point are only (20–30)° above ambient in all cases studied, the coefficients are constants to within 20%,[94] permitting us to ignore their spatial variation.

If we then ignore the z dependence of the coefficients, the analysis simplifies considerably. The coefficients (D11)–(D14) are constant, evaluated at an effective field $\bar{E}$ and temperature $\bar{T}$, defined in the following manner: For radially uniform solutions $E(z)$, $T(z)$ of Eqs. (D1)–(D6), at a given total current I and voltage V, we define

$$\bar{E} \equiv (V/d) = (1/d)\int_{-d/2}^{d/2} E(z)\,dz$$

and $\bar{T}$ such that

$$I = \pi R^2 \sigma(T) E\, e^{|\bar{E}|/E_0}\,.$$

The inhomogeneous term on the right-hand side of (D10) drops out and we are left with a coupled pair of linear inhomogeneous elliptic partial differential equations, whose solutions may be obtained in closed form.

As seen in Appendix C, an inhomogeneous system of equations will possess a solution only if certain solvability conditions are satisfied. The homogeneous form of the above system is self-adjoint if a weight factor of

$$\frac{1}{\sigma}\frac{\partial\sigma}{\partial T}\frac{1}{2+E/E_0}$$

is used in Eq. (D9), so that the solvability criterion for this system may be determined as follows. Multiply

$$K\nabla^2 T' - E\frac{2+E/E_0}{1+E/E_0}\frac{\psi_r'}{r} - \frac{\partial\sigma}{\partial T}\frac{E^2}{1+E/E_0}T' - f(r,z) = 0 \tag{D15}$$

by

$$\frac{1}{\sigma}\frac{\partial\sigma}{\partial T}\frac{1}{2+E/E_0}\tilde{T}\,,$$

where $\tilde{T}$ is a solution of the homogeneous form of (D15) when the coefficients are evaluated at $\bar{E}$ and $\bar{T}$, and add to this the product of

$$\frac{\partial}{\partial r}\left(\frac{1}{\sigma(1+E/E_0)}\frac{\psi_r'}{r} + \frac{1}{\sigma}\frac{\partial\sigma}{\partial T}\frac{ET'}{1+E/E_0}\right) + \frac{\partial}{\partial z}\left(\frac{\psi_z'}{r\sigma}\right) - g(r,z) = 0\,, \tag{D16}$$

with $\tilde{\psi}(r,z)/r$ where $\tilde{\psi}$ is a solution of the homogeneous form of (D16). Integrating by parts, using the fact that the system is self-adjoint and that $\tilde{T}$ and $\tilde{\psi}$ are solutions of the homogeneous forms of (D15) and (D16), respectively, we get the requirement

$$\int_0^R r\,dr\int_{-d/2}^{d/2} dz\left(\frac{1}{\sigma}\frac{\partial\sigma}{\partial T}\frac{1}{2+E/E_0}f(r,z)\tilde{T} + g(r,z)\frac{\tilde{\psi}}{r}\right) = 0\,, \tag{D17}$$

which must be satisfied if the inhomogeneous system (D15) and (D16) is to have a solution.

The solution of the homogeneous problem may be obtained by separation of variables. Proceeding in this manner, we find that

$$T'(r,z) = J_0(kr)T'(z)$$

for k such that $J_1(kR) = 0$. Substituting this in (D9) we get

$$\frac{\psi_r'(r)}{rJ_0(kr)} = \frac{1}{A\psi'(z)}\left\{K\left(\frac{d^2}{dz^2} - k^2\right) - B\right\}T'(z) = \gamma\,,$$

so that

$$\psi'(r,z) = \frac{\gamma}{k}rJ_1(kr)\psi'(z)\,.$$

We are left with the coupled pair of equations

$$\gamma A\psi'(z) = K\left(\frac{d^2}{dz^2} - k^2\right)T'(z) - BT'(z)\,, \tag{D18}$$

$$\frac{\gamma}{\sigma}\frac{d^2}{dz^2}\psi'(z) - \gamma Ck^2\psi'(z) - k^2DT'(z) = 0\,. \tag{D19}$$

Eliminating $\psi'(z)$, $T'(z)$ satisfies

$$\frac{d^4T'}{dz^4} - \left(k^2 + \frac{B}{K} + Ck^2\sigma\right)\frac{d^2T'}{dz^2} + \left(k^4\sigma C + \frac{k^2CB\sigma}{K} - \frac{k^2DA\sigma}{K}\right)T' = 0\,, \tag{D20}$$

$$T'(\pm\tfrac{1}{2}d) = 0\,,$$

$$\left[\frac{d^3}{dz^3}T' - \left(k^2 + \frac{B}{K}\right)\frac{d}{dz}T'\right]\Bigg|_{\pm d/2} = 0\,. \tag{D21}$$

If we let

$$\beta = k^2 + \frac{B}{K} + Ck^2\sigma = k^2\frac{2+E/E_0}{1+E/E_0} + \frac{E^2}{K}\left(\frac{\partial\sigma}{\partial T}\Big/(1+E/E_0)\right)$$

and

$$\delta = \sigma Ck^4 + \frac{k^2CB\sigma}{K} - \frac{k^2DA\sigma}{K} = \frac{k^4}{1+E/E_0} - \frac{\partial\sigma}{\partial T}\frac{k^2}{K}\frac{E^2}{1+E/E_0}\,,$$

then (C20) has the solution

$$T'(z) = \eta\cosh q_1 z + \nu\cos q_2 z$$

where

$$q_1^2 = \tfrac{1}{2}[\beta + (\beta^2 - 4\delta)^{1/2}] \quad \text{and} \quad q_2^2 = \tfrac{1}{2}[(\beta^2 - 4\delta)^{1/2} - \beta],$$

and η and ν are arbitrary.

Utilizing the first boundary condition $T'(\pm\frac{1}{2}d) = 0$,

$$T'(z) = \eta\left[\cosh q_1 z - \frac{\cosh \frac{1}{2}q_1 d}{\cos \frac{1}{2}q_2 d}\cos q_2 z\right].$$

The secondary boundary condition now determines the bifurcation points, i.e., the $\bar{T}, \bar{E}$ for which solutions to (D9) and (D10) exist. Equation (D21) requires that q_1 and q_2 must satisfy the transcendental equation

$$\left(q_1^2 q_2 - \frac{k^2 q_2}{1 + E/E_0}\right)\cosh \tfrac{1}{2}q_1 d \sin \tfrac{1}{2}q_2 d + \left(q_1 q_2^2 - \frac{k^2 q_1}{1 + E/E_0}\right)\sinh \tfrac{1}{2}q_1 d \cos \tfrac{1}{2}q_2 d = 0 \tag{D22}$$

which is in fact a condition on $\bar{E}$, $\bar{T}$, k being known.

Finally, $\psi'(z)$ is determined by (D18) to be

$$\psi'(z) = \eta\left(\frac{K(q_1^2 - k^2) - B}{\gamma A}\cosh q_1 z + \frac{\cosh \frac{1}{2}q_1 d}{\cos \frac{1}{2}q_2 d}\,\frac{K(q_2^2 + k^2) + B}{\gamma A}\cos q_2 z\right).$$

The particular solution to (D9) is easily seen to be

$$T'(z) = (A\alpha'/B)(1 - \operatorname{sech} \tfrac{1}{2}q_3 d \cosh q_3 z),$$

where

$$q_3^2 = B/K.$$

Since the solvability criterion (D17) is trivially satisfied because the right-hand side of (D9) is a constant, and $T(r) \sim J_0(kr)$, the full solution of Eqs. (D9) and (D10) is

$$T'(r, z) = \eta J_0(kr)\left(\cosh q_1 z - \frac{\cosh \frac{1}{2}q_1 d}{\cos \frac{1}{2}q_2 d}\cos q_2 z\right) + \frac{A\alpha'}{B}\left(1 - \operatorname{sech} \tfrac{1}{2}q_3 d \cosh q_3 z\right), \tag{D23}$$

$$\psi'(r, z) = \eta r J_1(kr)\left(\frac{K(q_1^2 - k^2) - B}{kA}\cosh q_1 z + \frac{\cosh \frac{1}{2}q_1 d}{\cos \frac{1}{2}q_2 d}\,\frac{K(q_2^2 + k^2) + B}{kA}\cos q_2 z\right), \tag{D24}$$

where α' is as yet undetermined. By choosing a suitable normalization for the general solutions of the homogeneous system, $T'(r, z)$ and $\psi'(r, z)$ are uniquely determined (see Appendix C). We will here let $\eta = -1$.

As in the case of the simpler model considered in Appendix C, a sequence of solutions $T_{mn}(r, z)$ and $\psi_{mn}(r, z)$ are defined in this manner, where the m-nth pair corresponds to the mth eigenvalue k_m and the nth eigenvalue determined by (D22). For $m = 1$ and $n = 1$, the solutions have no nodes in either the r or z direction. For general m and n, the solutions will possess $m - 1$ and $n - 1$ nodes in the r and z directions, respectively. With $\bar{E}$ and $\bar{T}$ defined as above, Eq. (D22) and the requirement that $J_1(kR) = 0$ suffice to determine the bifurcation points on the I-V characteristic. The solution set that we shall be primarily concerned with is $T_{11}(r, z)$, $\psi_{11}(r, z)$ corresponding to the lowest mode. For the choice $\eta = -1$, this mode decreases monotonically as a function of r and z for $r \in (0, R)$, $z \in (-\frac{1}{2}d, \frac{1}{2}d)$ and corresponds to a solution with a hot spot in the device center. The bifurcation point for this solution lies lowest on the I-V characteristic, closest to the voltage turnaround. The bifurcation points for the higher modes lie at progressively higher currents, their precise order, number, and location depending in detail on K, $\sigma(T, E)$, the device radius and thickness.

Differentiating Eqs. (D1)–(D6) twice with respect to ϵ and setting $\epsilon = 0$ we get

$$K\nabla^2 T'' - E\frac{2 + E/E_0}{1 + E/E_0}\frac{\psi_r''}{r} - \left(\frac{\partial\sigma}{\partial T}E^2 T''\Big/(1 + E/E_0)\right) = -E\frac{2 + E/E_0}{1 + E/E_0}\alpha'' - \left[\left(\frac{\partial\sigma}{\partial T}\right)^2\right]\sigma^{-1}\left(\frac{2 + 2E/E_0 + E^2/E_0^2}{(1 + E/E_0)^2} - \frac{\partial^2\sigma}{\partial T^2}\right)$$
$$\times \frac{E^2 T'^2}{1 + E/E_0} - \frac{1}{\sigma}\frac{\psi_z'^2}{r^2}\frac{2 + E/E_0}{1 + E/E_0} - \frac{1}{\sigma(1 + E/E_0)}\frac{2 + 2E/E_0 + E^2/E_0^2}{(1 + E/E_0)^2}\left(\alpha' - \frac{\psi_r'}{r}\right)^2 + \left[2\frac{\partial\sigma}{\partial T}E\Big/\sigma\left(1 + \frac{E}{E_0}\right)\right]$$
$$\times \left[\frac{2 + 2E/E_0 + E^2/E_0^2}{(1 + E/E_0)^2}\right]\left(\alpha' - \frac{\psi_r'}{r}\right)T', \tag{D25}$$

$$\frac{\partial}{\partial r}\left[\left(\frac{\psi_r''}{r} + \frac{\partial\sigma}{\partial T}ET''\right)\Big/\sigma(1 + E/E_0)\right] + \frac{\partial}{\partial z}\frac{\psi_z''}{r\sigma}$$
$$= \frac{\partial}{\partial r}\left(\left[-\frac{1}{\sigma E_0}\frac{\psi_z'^2}{r^2} - \frac{2 + E/E_0}{\sigma E_0(1 + E/E_0)}\left(\alpha' - \frac{\psi_r'}{r}\right)^2 + E\left\{\left[\left(\frac{\partial\sigma}{\partial T}\right)^2\Big/\sigma\right]\frac{2 + 2E/E_0 + E^2/E_0^2}{(1 + E/E_0)^2} - \frac{\partial^2\sigma}{\partial T^2}\right\}\right]\Big/\sigma\left(1 + \frac{E}{E_0}\right)\right)$$

$$-2\left[\frac{\partial\sigma}{\partial T}\Big/\sigma\left(1+\frac{E}{E_0}\right)\right]T'\left(\alpha'-\frac{\psi_r'}{r}\right)\Big/\sigma\left(1+\frac{E}{E_0}\right)\Big)+\frac{\partial}{\partial z}\left[\frac{2}{E_0}\,\frac{\psi_z'}{r}\left(\alpha'-\frac{\psi_r'}{r}+\frac{\partial\sigma}{\partial T}E_0T'\right)\Big/\sigma^2\left(1+\frac{E}{E_0}\right)\right], \tag{D26}$$

where the coefficients are evaluated at $\bar{E}$, $\bar{T}$. This is a linear inhomogeneous boundary-value problem for T'' and ψ'' in which the coefficients of the left-hand side are the same as in Eqs. (D9) and (D10). It will have a solution for some $\bar{E}$, $\bar{T}$ if the solvability condition (D17) is satisfied. In this way, α' is uniquely determined.

Once α' is determined in this manner, (D25) and (D26) could be solved for ψ'' and T''. This process may be continued to arbitrary order, establishing the existence of a set of solutions to Eqs. (D1)–(D6) corresponding to radially dependent temperature and field distributions in a neighborhood of the bifurcation points, provided that $\bar{E}$ and $\bar{T}$ exist such that (D22) is satisfied. These solutions bifurcate from the critical values of I and V corresponding to a certain $\bar{E}$ and $\bar{T}$, and their behavior in a neighborhood of these points is described by

$$T(r, z, \epsilon) = T(z) + \epsilon T'(r, z) + \tfrac{1}{2}\epsilon^2 T''(r, z) + \cdots,$$

$$\psi(r, z, \epsilon) = -(\alpha_0 + \epsilon'\alpha + \tfrac{1}{2}\epsilon^2\alpha'' + \cdots)\tfrac{1}{2}r^2 + \epsilon\psi'(r, z) + \tfrac{1}{2}\epsilon^2\psi''(r, z) + \cdots.$$

Bifurcation is possible only if the I-V characteristic corresponding to the radially uniform solutions possesses a region in which $dI/dv < 0$. The critical points lie in this break-back region, their exact position depending upon domain dimensions, K and σ.

Finally, the above results permit us to expand the electrostatic potential $\phi(r, z)$ in a Taylor series in ϵ about the critical points. For later reference, we note that if we let

$$\phi(r, z) = \phi(z) + \epsilon\phi'(r, z) + \tfrac{1}{2}\epsilon^2\phi''(r, z) + \cdots,$$

$$\frac{d\phi'}{dz} = \left(\alpha' - \frac{\psi_r'}{r} - \frac{\partial\sigma}{\partial T}ET'\right)\Big/\sigma\left(1+\frac{E}{E_0}\right),$$

so that the first-order change in potential along a bifurcation branch is

$$V' = \int_{-d/2}^{d/2}\frac{d\phi'}{dz}\,dz = \frac{\alpha' d}{\sigma}\left(\frac{2}{dq_3}\,\frac{2+E/E_0}{1+E/E_0}\tanh\tfrac{1}{2}q_3 d - 1\right).$$

APPENDIX E

We wish to investigate the stability with respect to infinitesimal perturbations of steady-state solutions of the time-dependent system

$$C\frac{\partial T}{\partial t} = \vec{\nabla}\cdot(K\vec{\nabla}T) + \vec{j}\cdot\vec{E}, \tag{E1}$$

$$\vec{j} = \sigma(T, E)\vec{E}, \tag{E2}$$

Maxwell's Equations, (E3)

Boundary Conditions. (E4)

We shall concern ourselves here with readily obtainable analytic results concerning radially uniform solutions and solutions derived in Appendices C and D, valid in an infinitesimal neighborhood of the bifurcation points.

In particular, we shall investigate the behavior of Eqs. (E1)–(E4) with respect to perturbations which keep the total current through the active region constant. This is equivalent to the physical situation of an infinite load resistance and corresponds to the most stable circuit configuration. We ignore possible "circuit" effects of stray capacitances and inductances, and thus limit consideration to the question of "model device" stability in an idealized situation.[69] It will be clear how to generalize the following for finite load resistances.

A. Analysis of model *B*

In this case (E1) reduces to the time-dependent form of (C1),

$$C\frac{\partial T}{\partial t} = \frac{1}{r}\frac{\partial}{\partial r}\left(rK\frac{\partial T}{\partial r}\right) - \frac{8K}{d^2}(T - T_0) + \sigma(T, E)E^2 \tag{E5}$$

$$T(0)\,(\text{finite}),\quad \left.\frac{dT}{dr}\right|_R = 0.$$

The current conservation equation is

$$I = \text{const} = \int_0^R r\,dr\left(\sigma(T, E)E_z + \frac{\epsilon}{4\pi}\frac{\partial E_z}{\partial t}\right) \tag{E6}$$

and the relevant Maxwell's equations are

$$\vec{\nabla}\times\vec{H} = \frac{4\pi}{c}\vec{j} + \frac{\epsilon}{c}\frac{\partial E}{\partial t}, \tag{E7}$$

$$\vec{\nabla}\times\vec{E} = -\frac{1}{c}\frac{\partial\vec{B}}{\partial t}. \tag{E8}$$

We may eliminate the magnetic field in (E7) and (E8) obtaining

$$\vec{\nabla}\times(\vec{\nabla}\times\vec{E}) = -\frac{4\pi\mu}{c^2}\frac{\partial\vec{j}}{\partial t} + \frac{\epsilon\mu}{c^2}\frac{\partial^2\vec{E}}{\partial t^2},$$

which reduces for this model system to

$$\frac{1}{r}\frac{\partial}{\partial r}\left(r\frac{\partial E_z}{\partial r}\right) = \frac{4\pi\mu}{c^2}\frac{\partial j_z}{\partial t} + \frac{\epsilon\mu}{c^2}\frac{\partial^2 E_z}{\partial t^2}, \tag{E9}$$

$$\frac{\epsilon}{4\pi}\frac{\partial E_r}{\partial t} + j_r = 0. \tag{E10}$$

Linearizing Eqs. (E5)–(E10) about some steady-state solutions $T(r)$, E while taking K a constant, we obtain

$$C\frac{\partial \delta T}{\partial t}=\frac{K}{r}\frac{\partial}{\partial r}\left(r\frac{\partial \delta T}{\partial r}\right)-\frac{8K}{d^2}\delta T+\frac{\partial \sigma}{\partial T}E^2\delta T+\left(2+\frac{E}{E_0}\right)\sigma(T,E)E\delta E_z, \tag{E11}$$

$$\int_0^R r\,dr\left[\frac{\partial \sigma}{\partial T}E\delta T+\sigma(T,E)\left(1+\frac{E}{E_0}\right)\delta E_z+\frac{\sigma(T,E)}{E_0}E\delta E_r+\frac{\epsilon}{4\pi}\frac{\partial}{\partial t}\delta E_z\right]=0, \tag{E12}$$

$$\frac{1}{r}\frac{\partial}{\partial r}\left(r\frac{\partial \delta E_z}{\partial r}\right)=\frac{4\pi\mu}{c^2}\frac{\partial}{\partial t}\left[\frac{\partial \sigma}{\partial T}E\delta T+\sigma\left(1+\frac{E}{E_0}\right)\delta E_z+\frac{\sigma(T,E)}{E_0}E\delta E_r\right]+\frac{\epsilon\mu}{c^2}\frac{\partial^2}{\partial t^2}\delta E_z, \tag{E13}$$

$$\frac{\epsilon}{4\pi}\frac{\partial \delta E_r}{\partial t}+\sigma\delta E_r=0, \tag{E14}$$

$$\left.\frac{\partial \delta T}{\partial r}\right|_R=0, \quad \text{and} \quad \delta E_r|_R=0. \tag{E15}$$

The above system of equations is separable, so that the time dependences in both δT and δE is given by $e^{\omega t}$. Substituting $\delta E_r(r,t)=\delta E_r(r)e^{\omega t}$ in (E14) it is clear that $\delta E_r\equiv 0$, so that Eqs. (E11)–(E15) may be rewritten

$$\frac{K}{r}\frac{d}{dr}\left(r\frac{d\delta T}{dr}\right)+\left(\frac{\partial \sigma}{\partial T}E^2-\frac{8K}{d^2}-C\omega\right)\delta T+\sigma E\left(2+\frac{E}{E_0}\right)\delta E_z=0, \tag{E16}$$

$$\int_0^R r\,dr\left\{\frac{\partial \sigma}{\partial T}E\delta T+\left[\sigma\left(1+\frac{E}{E_0}\right)+\frac{\epsilon\omega}{4\pi}\right]\delta E_z\right\}=0, \tag{E17}$$

$$\frac{1}{r}\frac{d}{dr}\left(r\frac{d\delta E_z}{dr}\right)=\frac{4\pi\mu}{c}\omega\left[\frac{\partial \sigma}{\partial T}E\delta T+\sigma\left(1+\frac{E}{E_0}\right)\delta E_z\right]+\frac{\epsilon\mu}{c^2}\omega^2\delta E_z. \tag{E18}$$

We now use Eqs. (E16)–(E18) to investigate the stability of the solutions $T(r,\theta)$,[95] $E(\theta)$ derived in Appendix C. It is clear, in this case, that ω, δT, and δE_z depend parametrically on θ, so that the most convenient way to proceed is to represent $\omega(\theta)$, $\delta T(\theta)$, and $\delta E_z(\theta)$ as a Taylor series in θ. Doing so, we get the lowest-order term in the expansion for ω, δT, and δE_z by setting $\theta=0$ in Eqs. (E16)–(E18). We use the notation of Appendix C, in which $T(r,\theta)$ and $E(\theta)$ are given by (C3) and (C4), and write

$$\delta T(r,\theta)=\delta T(r)+\theta\delta T'(r)+\frac{\theta^2}{2}\delta T''(r)+\cdots, \tag{E19}$$

$$\omega(\theta)=\omega+\theta\omega'+\tfrac{1}{2}\theta^2\omega''+\cdots, \tag{E20}$$

$$\delta E_z(r,\theta)=\delta E_z(r)+\theta\delta E_z'(r)+\tfrac{1}{2}\theta^2\delta E_z''+\cdots. \tag{E21}$$

Setting $\theta=0$, the coefficients in Eqs. (E16)–(E18) are independent of r, T, and E being solutions of

$$-\alpha(T-T_0)+\sigma(T,E)E^2=0.$$

Equations (E17) and (E18) imply that $(d\delta E_z/dr)|_R=0$, so that solutions of the above system are

$$\delta T(r)=a\phi_0(l_j r)=a\beta J_0(l_j r), \quad \beta^2=(2/R^2)[1/J_0^2(l_j R)]$$

$$\delta E_z(r)=b\phi_0(l_j r)$$

where the l_j are such that $J_1(l_j R)=0$ and

$$b=\left[Kl_j^2-\left(\frac{\partial \sigma}{\partial T}E^2-\frac{8K}{d^2}-C\omega\right)\right]\Big/\sigma E\left(2+\frac{E}{E_0}\right). \tag{E22}$$

In addition, ω must satisfy the equation

$$c\omega^3+d\omega^2+e\omega+f=0, \tag{E23}$$

where

$$c=\frac{\mu\epsilon}{c^2}C,$$

$$d=\frac{\epsilon\mu}{c^2}\left[Kl_j^2-\left(\frac{\partial \sigma}{\partial T}E^2-\frac{8K}{d^2}\right)\right]+\frac{4\pi\mu}{c^2}\sigma\left(1+\frac{E}{E_0}\right)C,$$

$$e=\frac{4\pi\mu}{c^2}\left[\sigma\left(1+\frac{E}{E_0}\right)\left(Kl_j^2+\frac{8K}{d^2}\right)+\sigma\frac{\partial \sigma}{\partial T}E^2\right]+Cl_j^2,$$

$$d=l_j^2\left[Kl_j^2-\left(\frac{\partial \sigma}{\partial T}E^2-\frac{8K}{d^2}\right)\right].$$

Note that if $Kl_j^2>(\partial\sigma/\partial T)E^2-\alpha$, every coefficient in (E23) is real and greater than zero so that there can be no real roots greater than zero. Assuming there exists a complex pair of solutions $\omega=\zeta+i\xi$ it may be shown that the equation satisfied by ζ is of the form (E23) with all coefficients real and greater than zero, so that there are no such roots with $\zeta\geq 0$. Therefore all the roots of (E23) have negative real parts. If $Kl_j^2=(\partial\sigma/\partial T)E^2-\alpha$, one of the roots of (E23) is zero, and the other two have negative real parts. If $Kl_j^2>(\partial\sigma/\partial T)E^2-\alpha$, similar arguments show that the real root is greater than zero.

It has been shown in Appendix C that a sequence of bifurcation points determined by the eigenvalues $k_n^2=1/K[(\partial\sigma/\partial T)E^2-\alpha]$ exists along the negative differential conductivity portion of the I-V characteristic, the first one, at k_1, lying nearest

the voltage turnaround (Fig. 23). Therefore, $T_n(r, \theta)$ is unstable for θ sufficiently small unless k_n is the smallest eigenvalue, so that all the solutions bifurcating from the radially uniform branch of the characteristic at $k_j, j > 1$ in Fig. 23 are unstable, at least in a small neighborhood of their respective bifurcation points, with respect to perturbations of the form $\delta T(r) = \phi_0(k_i r)$, $i < j$. Clearly (E23) also shows that the radially uniform branch of the characteristic is unstable (stable) above (below) the lowest bifurcation point, i.e., when

$$\frac{1}{K}\left(\frac{\partial\sigma}{\partial T}E^2 - \alpha\right) > (<)\ l_1^2 .$$

For $(1/K)[(\partial\sigma/\sigma T)E^2 - \alpha] = k_1^2$ and $l_j = l_1$, we get $\omega = 0$, so that we must proceed to the next highest order in θ to determine the stability of the branch bifurcating at k_1. First, note that $\omega = 0$ implies $\delta E_z(r) = 0$ because of (E22).

Differentiating Eqs. (E16)–(E18) once with respect to θ and setting $\theta = 0$:

$$\frac{1}{r}\frac{d}{dr}\left(r\frac{d\delta T'}{dr}\right) + \frac{1}{K}\left(\frac{\partial\sigma}{\partial T}E^2 - \alpha\right)\delta T' + \frac{1}{K}\left(2 + \frac{E}{E_0}\right)\sigma E\delta E_z' + \frac{1}{K}\left[\frac{\partial^2\sigma}{\partial T^2}E^2 T' + \frac{\partial\sigma}{\partial T}\left(2 + \frac{E}{E_0}\right)EE' - C\omega'\right]\delta T = 0, \tag{E24}$$

$$\int_0^R r\,dr\left[\frac{\partial^2\sigma}{\partial T^2}ET'\delta T + \frac{\partial\sigma}{\partial T}E\delta T' + \left(1 + \frac{E}{E_0}\right)\sigma\delta E_z'\right] = 0, \tag{E25}$$

$$\frac{1}{r}\frac{d}{dr}\left(r\frac{d\delta E_z'}{dr}\right) = \frac{4\pi\mu}{c^2}\omega'\frac{\partial\sigma}{\partial T}E\delta T, \tag{E26}$$

where

$$T'(r) = \phi_0(kr) - \frac{\sigma E(2 + E/E_0)}{Kk_1^2}E_1',$$

and E_1', given by (C15), is independent of r. (E26) implies that

$$\delta E_z'(r) = \gamma\phi_0(k_1 r) + \eta,$$

where

$$\gamma = -\frac{4\pi\mu}{c}\omega'\frac{\partial\sigma}{\partial T}E\frac{1}{k_1^2}a$$

and η, is determined by (E25). Substituting these results into (E24), we get the equation

$$\frac{1}{r}\frac{d}{dr}\left(r\frac{d\delta T'}{dr}\right) + k_1^2\delta T' = -\frac{1}{K}\left[\frac{\partial^2\sigma}{\partial T^2}E^2T' + \frac{\partial\sigma}{\partial T}\left(2 + \frac{E}{E_0}\right)EE' - C\omega'\right] \times a\phi_0(k_1 r) - \frac{1}{K}\left(2 + \frac{E}{E_0}\right)\sigma E\left[\gamma\phi_0(k_1 r) + \eta\right],$$

which has a solution only if the right side is orthogonal to $r\phi_0(k_1 r)$ (see Appendix C). This solvability criterion determines ω':

$$\omega' = \left\{\frac{\partial^2\sigma}{\partial T^2}E^2\int_0^R \phi_0^3(k_1 r)r\,dr + \left(2 + \frac{E}{E_0}\right)E\frac{\partial\sigma}{\partial T}\left[1 - \left(\frac{\partial^2\sigma}{\partial T^2}\Big/\frac{\partial\sigma}{\partial T}\right)\frac{\sigma E^2}{Kk_1^2}\right]E'\right\} \times \left[C + \frac{4\pi\mu}{c}\frac{\partial\sigma}{\partial T}\frac{\sigma E^2}{Kk_1^2}\left(2 + \frac{E}{E_0}\right)\right]^{-1}.$$

Note that the last term in the square brackets is always positive, and

$$\int_0^R r\phi_0^3(k_1 r)\,dr = \tfrac{4}{3}(1/k_1^2)\int_0^{k_1 R}\phi_1^3(z)\,dz > 0.$$

For $\theta > 0$, if $\omega' < 0$, the branch bifurcating at the wave vector k_1 is stable in the immediate neighborhood of the bifurcation point in which the linear theory is correct, and unstable if $\omega' > 0$.

The analysis may be carried out in this manner to arbitrary order.

B. Analysis of model *A*

If one reviews the analysis of part A of this Appendix, it becomes clear that the displacement current effect does not influence the answer to the question of infinitesimal temporal stability of some branch of the *I-V* characteristic. The same results would have been obtained had we used

$$\vec{\nabla}\times\vec{H} = (4\pi/c)\vec{j}$$

instead of (E7). The reason for this lies in the fact that curl $\delta\vec{E} \sim \omega$, so that at points of neutral stability, $\omega = 0$, and curl $\delta\vec{E} = 0$. The signature of ω on either side of the point of neutral stability is not changed by the introduction of displacement current effects.[74]

The analysis of this section may be simplified enormously if we make use of this fact. Although it is still possible to carry out the full analysis as in part A, the results are much more transparent and the arguments simpler if we ignore the displacement current, so that

$$\vec{\nabla}\cdot\vec{j} = 0.$$

With this assumption, the time-dependent system corresponding to Eqs. (D1)–(D6) is

$$C\frac{\partial T}{\partial t} = \vec{\nabla}\cdot(K\vec{\nabla}T) + \vec{j}\cdot\vec{E}, \tag{E27}$$

$$\vec{\nabla}\cdot\vec{j} = 0, \tag{E28}$$

$$\vec{j} = \sigma(T)E\exp(|E|/E_0), \tag{E29}$$

$$T|_{\pm d/2} = T_0, \quad \left.\frac{\partial T}{\partial r}\right|_R = 0, \tag{E30}$$

$$\vec{j}\cdot\hat{r}|_R = 0, \quad j_r|_{\pm d/2} = 0. \tag{E31}$$

j can again be represented in terms of a potential ψ, so that the boundary conditions of keeping the

total current through the device fixed is satisfied if we require $\psi(R) = \text{const} = -I/2\pi$.

Linearizing Eqs. (E27)–(E31) about some steady-state solution $T(r, z)$, $\psi(r, z)$, taking K a constant we obtain

$$C\frac{\partial \delta T}{\partial t} = K\nabla^2 \delta T + \frac{\psi_z}{r}\delta\phi_r + \phi_r\frac{\delta\psi_z}{r} - \frac{\psi_r}{r}\delta\phi_z - \phi_z\frac{\delta\psi_r}{r}, \tag{E32}$$

$$\frac{\partial}{\partial r}\delta\phi_z - \frac{\partial}{\partial z}\delta\phi_r = 0, \tag{E33}$$

where $\delta\psi$ and $\delta\phi$ are related by

$$\frac{\delta\psi_z}{r} = \frac{\partial\sigma}{\partial T}\phi_r \exp\left(\frac{(\phi_r^2+\phi_z^2)^{1/2}}{E_0}\right)\delta T + \sigma(T)\exp\left(\frac{(\phi_r^2+\phi_z^2)^{1/2}}{E_0}\right)\left[1+\frac{\phi_r^2}{E_0(\phi_r^2+\phi_z^2)^{1/2}}\right]\delta\phi_r + \sigma(T)\frac{\phi_r\phi_z}{E_0(\phi_r^2+\phi_z^2)^{1/2}}\exp\left(\frac{(\phi_r^2+\phi_z^2)^{1/2}}{E_0}\right)\delta\phi_z$$

$$-\frac{\delta\psi_r}{r} = \frac{\partial\sigma}{\partial T}\phi_z \exp\left(\frac{(\phi_r^2+\phi_z^2)^{1/2}}{E_0}\right)\delta T + \sigma(T)\exp\left(\frac{(\phi_r^2+\phi_z^2)^{1/2}}{E_0}\right)\left[1+\frac{\phi_z^2}{E_0(\phi_r^2+\phi_z^2)^{1/2}}\right]\delta\phi_z + \sigma(T)\frac{\phi_r\phi_z}{(\phi_r^2+\phi_z^2)^{1/2}}\exp\left(\frac{(\phi_r^2+\phi_z^2)^{1/2}}{E_0}\right)\delta\phi_r$$

We shall now use Eq. (E32) and (E33) to investigate the stability of the solutions $T(r, z, \epsilon)$, $\psi(r, z, \epsilon)$ derived in Appendix D. As in part A, we assume that ω, δT, and $\delta\psi$ depend continuously on the amplitude parameter ϵ so that they may be expanded in a Taylor series about $\epsilon = 0$. We use the notation of Appendix D in which $T(r, z, \epsilon)$ and $\psi(r, z, \epsilon)$ are given by (D7) and (D8), and write

$$\delta T(r, z, \epsilon) = \delta T(r, z) + \epsilon\delta T'(r, z) + \cdots,$$

$$\delta\psi(r, z, \epsilon) = \delta\psi(r, z) + \epsilon\delta\psi'(r, z) + \cdots,$$

so that, setting $\epsilon = 0$ in (E30) and (E31) we get

$$C\frac{\partial\delta T}{\partial t} = K\nabla^2\delta T - E\frac{2+E/E_0}{1+E/E_0}\frac{\delta\psi_r}{r} - \frac{\partial\sigma}{\partial T}\frac{E^2}{1+E/E_0}\delta T \tag{E34}$$

and

$$\frac{\partial}{\partial r}\left[\left(\frac{\delta\psi_r}{r}+\frac{\partial\sigma}{\partial T}E\delta T\right)\Big/\sigma\left(1+\frac{E}{E_0}\right)\right] + \frac{\partial}{\partial z}\frac{\partial\psi_z}{r\sigma} = 0, \tag{E35}$$

where the coefficients are evaluated at $\bar{E}$, $\bar{T}$ defined in Appendix D.

The time dependence of both δT and $\delta\psi$ is clearly given by $e^{\omega t}$ so that (E34) and (E35) become homogeneous forms of (D9) and (D10). The solutions are given by (D24) and the first term in (D23), provided (D22) is satisfied with the new definitions

$$\beta = l^2\frac{2+\bar{E}/E_0}{1+\bar{E}/E_0} + \frac{1}{K}\frac{\partial\sigma}{\partial T}(\bar{T}, \bar{E})\frac{\bar{E}^2}{1+\bar{E}/E_0} + \frac{C\omega}{K}, \tag{E36}$$

$$\delta = \frac{l^4}{1+\bar{E}/E_0} - \frac{\partial\sigma(\bar{T}, \bar{E})}{\partial T}\frac{l^2\bar{E}^2}{(1+\bar{E}/E_0)K} + \frac{C\omega k^2}{K(1+E/E_0)}, \tag{E37}$$

where l_j such that $J_1(l_j R) = 0$.

Let $\bar{E}^*$, $\bar{T}^*$ be the values of $\bar{E}$, $\bar{T}$ at the lowest bifurcation point determined in Appendix D. Let $\bar{E}'$, $\bar{T}'$ be values of $\bar{E}$, $\bar{T}$ at some point of the radially uniform I-V characteristic for a current greater than I_{11}, the current at the first bifurcation point. If $\bar{E}'$, $\bar{T}'$ lie at the m-nth bifurcation point, then Eqs. (E34)–(E37) clearly have solutions for $\omega > 0$. To see this, note that (D22) determines values of β' and δ' such that

$$\beta' = k_m^2\frac{2+\bar{E}'/E_0}{1+\bar{E}'/E_0} + \frac{1}{K}\frac{\partial\sigma}{\partial T}\frac{\bar{E}'^2}{1+\bar{E}'/E_0},$$

$$\delta' = \frac{k_m^4}{1+\bar{E}'/E_0} - \frac{1}{K}\frac{\partial\sigma}{\partial T}\frac{k_m^2\bar{E}'^2}{1+\bar{E}'/E_0},$$

so a solution to

$$\beta' = k_1^2\frac{2+\bar{E}^*/E_0}{1+\bar{E}^*/E_0} + \frac{1}{K}\frac{\partial\sigma}{\partial T}\frac{\bar{E}^{*2}}{1+\bar{E}^*/E_0} + \frac{C\omega}{K},$$

$$\delta' = \frac{k_1^2}{1+\bar{E}^*/E_0} - \frac{\partial\sigma}{\partial T}\frac{1}{K}\frac{k_1^2\bar{E}^{*2}}{1+\bar{E}^*/E_0} + \frac{C\omega k_1^2}{K(1+\bar{E}^*/E_0)}$$

exists for $\omega > 0$ since $k_1 \le k_m$, $k_m^2 < [\partial\sigma(\bar{T}', \bar{E})/\partial T]\bar{E}'^2/K$, and $\bar{E}' < \bar{E}^*$. In fact, for any $\bar{E}'$, $\bar{T}'$ defined above, it is easy to see in this way that (E36) and (E37) have solutions for $\omega > 0$, if we take $l = k_1$. Therefore, the portion of the I-V characteristic above the first bifurcation point is unstable as are all the branches bifurcating at the l-jth critical points, l, j not both 1, at least for ϵ small enough.

To this order we get no information concerning the stability of the branch bifurcating at the lowest critical point ($k = k_1$, $\bar{E} = \bar{E}_1^*$, $\bar{T} = \bar{T}_1^*$), since (E36) and (E37) have a solution for $\omega = 0$. To determine the stability of this branch we are required to proceed to the next highest order and calculate ω'.

Differentiating (E32) and (E33) once with respect to ϵ and setting $\epsilon = 0$ we get, remembering that $\omega = 0$,

$$K\nabla^2\delta T' - \frac{\frac{\partial\sigma}{\partial T}E^2}{1+E/E_0}\delta T' - E\frac{2+E/E_0}{1+E/E_0}\frac{\delta\psi_r'}{r} = \frac{E^2}{1+E/E_0}\left\{\frac{\partial^2\sigma}{\partial T^2}\left[\left(\frac{\partial\sigma}{\partial T}\right)^2\Big/\sigma\right]\frac{2+2E/E_0+E^2/E_0^2}{(1+E/E_0)^2}\right\}T'\delta T + C\omega'\delta T$$

$$+\left(\frac{\partial\sigma}{\partial T}\Big/\sigma\right)\frac{E}{(1+E/E_0)^3}(2+2E/E_0+E^2/E_0^2)\left[\left(\alpha'-\frac{\psi_r'}{r}\right)\delta T-\frac{\delta\psi_r}{r}T'\right]+\frac{2+2E/E_0+E^2/E_0^2}{\sigma(1+E/E_0)^2}\left(\alpha'+\frac{\psi_r'}{r}\right)\frac{\delta\psi_r}{r}$$

$$-\frac{2+E/E_0}{1+E/E_0}\frac{\psi_z'\delta\psi_z}{r^2\sigma},$$

$$\frac{\partial}{\partial r}\left[\left(\frac{\delta\psi_r'}{r}+\frac{\partial\sigma}{\partial T}E\delta T'\right)\Big/\sigma\left(1+\frac{E}{E_0}\right)\right]+\frac{\partial}{\partial z}\left\{\frac{\delta\psi_z'}{r\sigma}\right\}$$

$$=\frac{\partial}{\partial r}\left\{\frac{-\left\{\frac{\partial^2\sigma}{\partial T^2}-\left[\left(\frac{\partial\sigma}{\partial T}\right)^2\Big/\sigma\right]\frac{2+2E/E_0+E^2/E_0^2}{(1+E/E_0)^2}\right\}ET'\delta T-\left(\frac{\partial\sigma}{\partial T}\Big/\sigma\right)\frac{1}{(1+E/E_0)^2}\left[\left(\alpha'-\frac{\psi_r'}{r}\right)\delta T-\frac{\delta\psi_r}{\sigma}T'\right]}{\sigma(1+E/E_0)}\right.$$

$$\left.+\frac{\frac{2+E/E_0}{\sigma E_0(1+E/E_0)^2}\left(\alpha'-\frac{\psi_r'}{r}\right)\frac{\delta\psi_r}{r}-\frac{1}{E_0}\frac{\delta\psi_z\psi_z'}{r^2\sigma}}{\sigma(1+E/E_0)}\right\}+\frac{\partial}{\partial z}\left\{\frac{\frac{\partial\sigma}{\partial T}}{\sigma^2(1+E/E_0)}\left[\delta T\frac{\psi_z'}{r}+T'\frac{\delta\psi_z}{r}\right]+\frac{1}{\sigma^2(1+E/E_0)}\right.$$

$$\left.\times\left[\left(\alpha'-\frac{\psi_r'}{r}\right)\frac{\delta\psi_r}{r}-\frac{\psi_z'}{r}\frac{\delta\psi_r}{r}\right]\right\},$$

where the coefficients are evaluated at $\bar{E}^*$, $\bar{T}^*$.

The solubility condition (D17) determines ω'. The branch of the I-V characteristic bifurcating at $\bar{E}^*$, $\bar{T}^*$, is stable or unstable in the neighborhood of this critical point, depending upon whether $\epsilon\omega'$ is less than or greater than zero.

*Research supported in part by ARO(D), and benefited from general support of Materials Science at The University of Chicago by ARPA and the NSF.

‡Submitted in partial satisfaction of the requirements for the Ph. D. degree in Physics at The University of Chicago.

†During the course of this work the author held a General Telephone and Electronics Fellowship.

Present address: Institut für Festkörperforschung, KFA Jülich, 517 Jülich, West Germany.

[1]Fundamentals of Amorphous Semiconductors, Report of the Ad Hoc Committee on the Fundamentals of Amorphous Semiconductors (National Academy of Sciences, Washington, D. C. 1972).

[2]S. R. Ovshinsky, Phys. Rev. Lett. 21, 1450 (1968).

[3]A. D. Pearson, W. R. Northover, J. F. Dewald, and W. F. Peck Jr., in *Advances in Glass Technology* (Plenum, New York, 1962), p. 357.

[4]D. Adler, CRC Critical Rev. Solid State Sci. 2, 317 (1971).

[5]R. R. Shanks, J. Non-Cryst. Solids 2, 504 (1970).

[6]H. Fritzsche, IBM J. Res. Devl. 13, 515 (1969).

[7]H. J. Stocker, Appl. Phys. Lett. 15, 55 (1969).

[8]H. Fritzsche, in *Proceedings of the International Conference on Conduction in Low-Mobility Materials*, edited by N. Klein, D. S. Tannhauser, and M. Pollack (Taylor and Francis, London, 1971).

[9]M. H. Cohen, R. G. Neale, and A. Paskin, J. Non-Cryst. Solids 8-10, 885 (1972).

[10]H. J. Stocker, C. A. Barlow, and D. F. Weirauch, J. Non-Cryst. Solids 4, 523 (1970).

[11]A. C. Warren, Electronics Lett. 5, 461, 609 (1969); J. Non-Cryst. Solids 4, 613 (1970).

[12]D. L. Thomas and A. C. Warren, Electronics Lett. 6, 62 (1970).

[13]A. C. Warren and J. C. Male, Electronics Lett. 6, 567 (1970).

[14]D. L. Thomas and J. C. Male, J. Non-Cryst. Solids 8-10, 522 (1972).

[15]H. S. Chen and T. T. Wang, Phys. Status Solidi A 2, 79 (1970).

[16]F. M. Collins, J. Non-Cryst. Solids 2, 496 (1970).

[17]P. Burton and R. W. Brander, Int. J. Electronics 27, 517 (1969).

[18]W. W. Sheng and C. R. Westgate, Solid State Commun. 9, 387 (1971).

[19]G. Dohler, Phys. Status Solidi A 1, 125 (1970).

[20]K. W. Boer and S. R. Ovshinsky, J. Appl. Phys. 41, 2675 (1970).

[21]K. W. Boer, G. Dohler, and S. R. Ovshinsky, J. Non-Cryst. Solids 4, 573 (1970).

[22]K. W. Boer, Phys. Status Solidi A 2, 817 (1970); Phys. Status Solidi A 4, 571 (1971).

[23]N. Croitoru, L. Vescan, C. Popescu, and Lazarescu, J. Non-Cryst. Solids 4, 493 (1970).

[24]N. Croitoru and C. Popescu, Phys. Status Solidi 3, 1047 (1970); Rev. Roum. Phys. 16, 129 (1971); J. Non-Cryst. Solids 8-10, 531 (1972).

[25]T. Kaplan and D. Adler, Appl. Phys. Lett. 19, 418 (1971); J. Non-Cryst. Solids 8-10, 538 (1972).

[26]J. M. Robertson and A. E. Owen, J. Non-Cryst. Solids 8-10, 439 (1972).

[27]A. H. M. Shousha, J. Appl. Phys. 42, 5131 (1971).

[28]N. F. Mott, Phil. Mag. 19, 835 (1969); Contemp. Phys. 10, 125 (1969).

[29]F. W. Schmidlin, Phys. Rev. B 1, 1583 (1970).

[30]H. K. Henisch, E. A. Fagen, and S. R. Ovshinsky, J. Non-Cryst. Solids 4, 538 (1970).

[31]S. R. Ovshinsky and H. Fritzsche, J. Non-Cryst. Solids 2, 393 (1970); J. Non-Cryst. Solids 4, 464 (1970).

[32]N. F. Mott, Phil. Mag. 24, 911 (1971).

[33]A brief summary of the results derived in this paper was presented at the Fourth International Conference on Amorphous and Liquid Semiconductors (Ref. 34).

[34]D. M. Kroll and M. H. Cohen, J. Non-Cryst. Solids 8-10, 544 (1972).

[35]For a summary of the earlier work in this field see Refs. 36–38.

[36]W. Franz, *Encyclopedia of Physics* (Springer, Berlin, 1956), Vol. 17, p. 155.

[37]N. Klein, in *Advan. Electr. Electron. Physics*, ed. by L. Morton (Academic, New York, 1969), Vol. 26, pp. 309–424.

[38]J. J. O'Dwyer, *The Theory of Dielectric Breakdown in Solids* (Oxford U. P., London, 1964).

[39]H. K. Rockstad, R. Flasck, and S. Iwasa, J. Non-Cryst. Solids 8-10, 326 (1972).

[40]S. C. Moss and J. P. deNeufville, J. Non-Cryst. Solids 8-10, 45 (1972).

[41]G. Busch, H. J. Guntherodt, H. V. Kunzi, and A. Schwiger, Phys. Lett. A 33, 64 (1970).

[42]J. C. Perron, J. Non-Cryst. Solids 8-10, 272 (1972).

[43]A. R. Regel, A. A. Andreev, and Mamadaliev, J. Non-Cryst. Solids 8-10, 455 (1972).

[44]R. W. Haisty and H. Krebs, J. Non-Cryst. Solids 1, 399, 427 (1969).

[45]J. C. Perron, Adv. Phys. 16, 657 (1967).

[46]J. C. Male, Electronics Lett. 6, 91 (1970).

[47]H. Fritzsche, Bussei (Japan) 13, 50 (1972).

[48]E. A. Fagen and H. Fritzsche, J. Non-Cryst. Solids 2, 170 (1970).

[49]P. J. Walsh *et al.*, J. Non-Cryst. Solids 2, 125 (1970).

[50]J. P. de Neufville (unpublished).

[51]J. C. Perron, Phys. Letters 32A, 169 (1970).

[52]R. G. Neale, J. Non-Cryst. Solids 2, 558 (1970).

[53]The coefficient $8K/d^2$ of the effective cooling term was chosen so that the I-V characteristic determined by radially uniform solutions of Fig. (7) coincides, at low current densities, with the I-V characteristic determined by radially uniform solutions of Eqs. (1)–(3) in model A (See Fig. 8).

[54]We wish to thank R. Landauer and F. Stern for pointing this work out to us. It appears that the Spenke work was the first to realize that the presence of thermally induced negative differential resistance could lead to the existence of more than one branch of the I-V characteristic.

[55]E. Spenke, Wiss. Veroff. Siemens-Werk. 15, 92 (1936); Arch. Electrotech. 30, 15 (1936).

[56]H. Lueder and E. Spenke, Z. Phys. 36, 36 (1935); Z. Techn. Physik 11, 373 (1935).

[57]H. Lueder, W. Schottky, and E. Spenke, Naturwissenschaften 24, 61 (1936).

[58]O. A. Ladyzhenskaya and N. N. Ural'tseva, *Linear and Quasilinear Elliptic Equations* (Academic, New York, 1968).

[59]All the results presented in this paper for model B were derived using $K_l = 4\text{mW/cm °K}$, $E_0 = 3.7\times10^4$ V/cm, $Ge_{15}Te_{81}X_4$ conductivity data (Fig. 2), Lorentz number 2.45×10^{-8} $W\Omega/°K^2$, and $d = 1\ \mu$, $R = 10\ \mu$, unless otherwise noted.

[60]R. W. Keyes, Comments on Solid State Phys. 4, 1 (1971).

[61]W. Kaplan, *Ordinary Differential Equations* (Addison-Wesley, Reading, Mass., 1962).

[62]In order for the system [Eqs. (35) and (36)] to possess two solutions $\lambda = \lambda_1, \lambda_2$, $\sigma(u)$ must possess a point of inflection for a $u' > u_0$, i.e., satisfy property A of Appendix B: $d\sigma/du \geq 0$ for $u > u_0$, $d^2\sigma(u')/du^2 = 0$ for some $u' > u_0$ and $d^2\sigma/du^2 \gtrless 0$ for $u \lesseqgtr u'$.

[63]In this segment of the analysis it is permissible to take the thermal conductivity K to be a constant, since for all the cases considered, the temperatures at the bifurcation points are all well below 500 °K, the temperature at which K begins to increase.

[64]M. H. Millman, in *Bifurcation Theory and Nonlinear Eigenvalue Problems*, edited by J. B. Keller and S. Antman (Courant Institute of Math. Sci., New York University, New York, 1968), p. 327.

[65]M. H. Millman and J. B. Keller, J. Math. Phys. 10, 342 (1969).

[66]J. B. Keller and Lu Ting, Commun. Pure Appl. Math. 19, 371 (1966).

[67]That such pairs of solutions exist can be seen by looking at the phase-plane plot in Fig. 9(b). For solutions which form closed orbits about b, one can either start at $r = 0$ to the right or to the left of b, the first correponds to $u(0)$ a maximum, the other to $u(0)$ a minimum.

[68]This point is essentially determined by the location of the voltage minimum attained at high currents by the I-V characteristic determined by radially uniform solutions of Eqs. (26)–(31).

[69]M. P. Shaw and I. J. Gastman, J. Non-Cryst. Solids 8-10, 999 (1972).

[70]M. P. Shaw, H. L. Grubin, and I. J. Gastman, IEEE Trans. Electron. Devices ED-20, 169 (1973).

[71]L. Altcheh, N. Klein, and I. Katz, J. Appl. Phys. 43, 3258 (1972).

[72]B. W. Knight and G. A. Peterson, Phys. Rev. 155, 393 (1967).

[73]In the Spenke work it was incorrectly assumed that the existence of a solution to the linearized problem was sufficient to establish the existence of another solution to the original equation (i.e., determine the bifurcation points). This condition is necessary but not sufficient. See Refs. 64 and 65.

[74]R. Landauer and J. W. F. Woo, Comments on Solid State Phys. 4, 139 (1972).

[75]M. Gunthersdorfer, J. Appl. Phys. 42, 2566 (1971).

[76]D. Armitage, D. E. Brodie, and P. C. Eastman, Can. J. Phys. 48, 2780 (1970).

[77]D. F. Weirauch, Appl. Phys. Lett. 16, 72 (1970).

[78]A. D. Pearson and C. E. Miller, Appl. Phys. Lett. 14, 280 (1969).

[79]B. T. Kolomiets, E. A. Lebedev, and I. A. Taksami, Sov. Phys.-Semicond. 3, 267 (1969).

[80]R. W. Pryor and H. K. Henisch, J. Non-Cryst. Solids 7, 181 (1972).

[81]H. K. Henisch, R. W. Pryor, and G. J. Vendura, Jr., J. Non-Cryst. Solids 8-10, 415 (1972).

[82]H. K. Henisch and R. W. Pryor, Solid State Electron. 14, 765 (1971).

[83]S. H. Lee and H. K. Henisch, Solid-State Electron. 16, 155 (1973).

[84]R. W. Pryor and H. K. Henisch, Appl. Phys. Lett. 18, 324 (1971).

[85]If one of the electrodes is a crystalline semiconductor this effect seems to be accentuated, at least when both pulses are of the same sign. See Ref. 89.

[86]Further results concerning prethreshold polarization effects may be found in W. D. Burgess and H. K. Henisch, Solid State Electron. 16, 15 (1973).

[87]The increase in delay time (equivalent to an increase in

V_{TH}) upon polarity reversal would be due to the time required to sweep out and change the sign of the free-space charge predicted by this theory. It appears even here though that this may not be the complete explanation (see Ref. 82).

[88]H. K. Henisch and G. J. Vendure Jr., Appl. Phys. Lett. 19, 363 (1971).

[89]G. J. Vendura Jr. and H. K. Henisch, J. Non-Cryst. Solids 11, 105 (1972).

[90]H. Stiegler and D. R. Haberland, J. Non-Cryst. Solids 11, 147 (1972).

[91]S. H. Lee, H. K. Henisch, and W. B. Burgess, J. Non-Cryst. Solids 8-10, 422 (1972).

[92]S. H. Lee and H. K. Henisch, J. Non-Cryst. Solids 11, 192 (1972).

[93]M. H. Cohen and R. G. Neale (unpublished); cf. S. R. Ovshinsky, Phys. Rev. Lett. 21, 1450 (1968).

[94]The fact that a strong field dependence of the conductivity will tend to flatten out the electric field distribution and therefore reduce the variation of $\sigma(T, E)$ as a function of z in the device interior has been noted previously (Ref. 22). It is this same effect which is the cause of the presence of the break-back region in the I-V characteristic determined by radially uniform solutions of Eqs. (D1)–(D6).

[95]Only in Subsection A of Appendix E we will denote the expansion parameter by θ in order to avoid confusion with the dielectric constant ϵ.